miRNAS IN EPITHELIAL MESENCHYMAL TRANSITION AND POSTERIOR CAPSULAR OPACIFICATION

by

Jocelyn C. Zajac

A thesis submitted to the Faculty of the University of Delaware in partial fulfillment of the requirements for the degree of Honors Degree in Biochemistry with Distinction

Spring 2013

miRNAS IN EPITHELIAL

MESENCHYMAL TRANSITION

AND POSTERIOR

CAPSULAR OPACIFICATION

by

Jocelyn C. Zajac

Approved: _____

Melinda K. Duncan, Ph.D
Professor in charge of thesis on behalf of the Advisory Committee

Approved: _____

Jia L. Song, Ph.D
Committee member from the Department of Biological Sciences

Approved: _____

Salil Lachke, Ph.D
Committee member from the Board of Senior Thesis Readers

Approved: _____

Michael Arnold, Ph.D.
Director, University Honors Program

ACKNOWLEDGMENTS

I would like to thank my thesis advisor Dr. Melinda Duncan, and all of my committee members for helping me accomplish a senior thesis. I would also like to express my gratitude to Abby Manthey and Fahmy Mamuya, two graduate students in the Duncan lab, for introducing me to a laboratory environment, and guiding me through the research process. Finally, I would like to acknowledge the support of the Howard Hughes Medical Institute, the National Eye Institute and the University of Delaware Undergraduate Research Program.

TABLE OF CONTENTS

LIST OF TABLES

LIST OF FIGURES

ABSTRACT

Cataract ensues when there is a deviation from normal lens development and/or maintenance (Chiu 2008). After extracapsular lens extraction surgery is performed to remove and replace the damaged tissue, a phenomenon known as posterior capsule opacification (PCO) occurs when any remaining cells proliferate and migrate to the posterior portion of the lens and undergo either epithelial-to-mesenchymal transition (EMT), or aberrant fiber cell differentiation (Wormstone et al., 2009). This wound healing process can result in poor visual acuity, and what is known as a "second cataract" (Spalton 2011). Two proteins known to upregulate during PCO were specifically studied to help determine their regulatory mechanisms during this phenomenon: Sip1 and αV integrin.

Smad Interacting Protein 1 (SIP1) is a transcription factor shown to have a vital role in embryonic development of several tissues of the eye and lens fiber cell maturation (Yoshimoto et al., 2005). Because SIP1 is able to repress epithelial gene expression and activate mesenchymal gene expression in other tissues (Andersen et al., 2005), it may also have a role in PCO. This study found that miRNAs of the miR200 family, which can regulate EMT, control cellular phenotype, and lead to the development of tumors (Bracken et al., 2012), are not present in appreciable levels in the lens, confirming that it is highly unlikely that PCO is under miR200 family control.

Other miRNAs may have a role in PCO, however. miR31 has been shown to be a master regulator of the expression of alpha V integrins (Augoff *et al*, 2011), transmembrane proteins that aids cell signaling, adhesion, migration, and organization (Tarone *et al*, 2000). Furthermore, αV integrin subunit protein upregulates during EMT even though its RNA does not (Mamuya and Duncan, 2012; Mamuya et al, unpublished). This led to the idea that miRNAs may control protein expression levels, which in turn may induce PCO. In this study, miR31 levels downregulate in wildtype lens cells 24 hours post-surgery. Furthermore, transforming growth factor induced (TGFβi), a target of TGFβ signaling elevates to a greater extent in WT than αV-null lens cells which is consistent with the fact that PCO does not occur in the αV integrin KO. To describe the proposed miR31 model during PCO briefly, decreased miR31 allows for increased αV integrin protein levels, which ultimately lead to increased TGFβi protein and induced EMT.

To date, many findings indicate a role for SIP1 and αV integrin in the development and maturation of the lens, as well as in wound healing, but there is little known about the regulation of gene expression in the lens, especially during PCO. This study addresses the question of how miRNA expression overlaps with protein expression, and how miRNAs may be involved in PCO.

Chapter 1

BACKGROUND AND SIGNIFICANCE

Mammalian Eye Development

The mammalian eye is a complex neurosensory organ (Li and Piatigorsky, 2009), and its multi-stage development requires multiple tissue interactions (Lang, 2004). One essential component of the eye is the lens, which is responsible for the light refraction necessary for high-resolution vision. Complete embryonic lens development is shown in Figure 1.

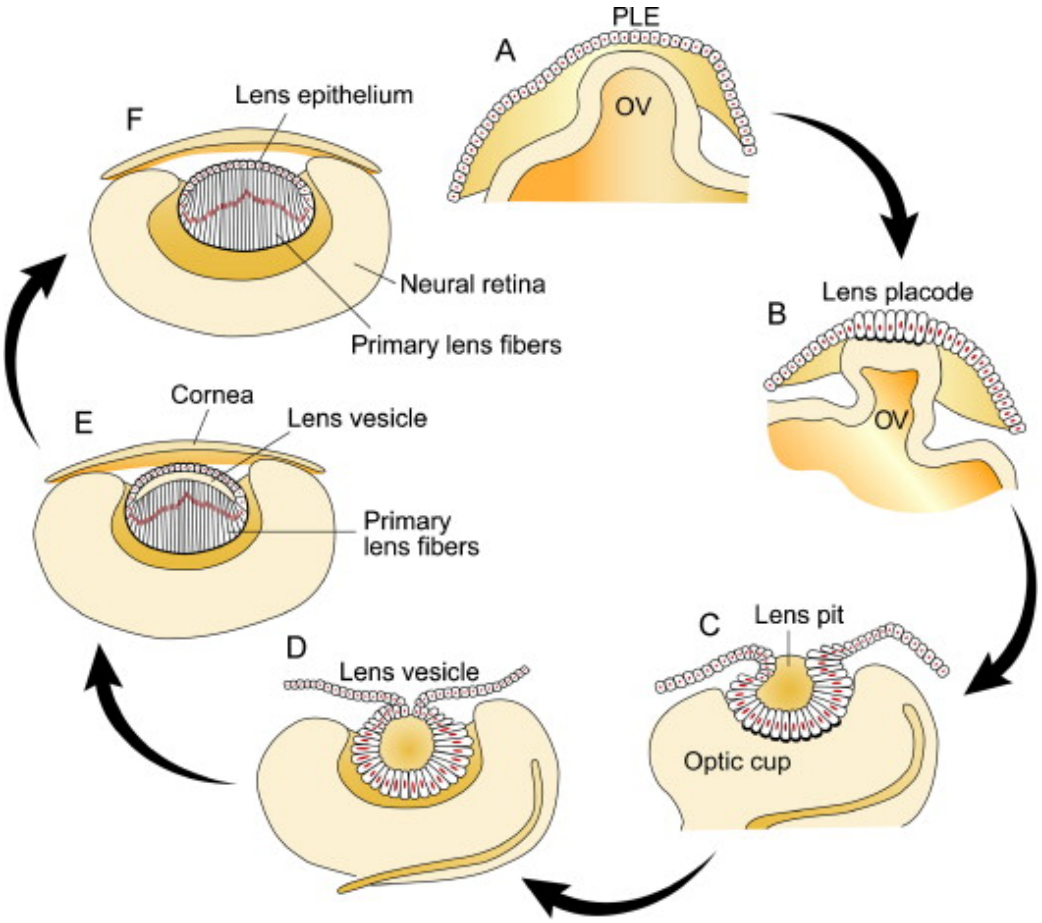

Figure 1 Embryonic development of the lens. (A) A sheet of surface ectoderm after being exposed to multiple inductive factors forms a presumptive lens ectoderm (PLE), which contacts the optical vesicle (OV) causing a thickening of the PLE to become the lens placode. (B,C) The lens placode invaginates to create the lens pit, which ultimately forms the lens vesicle. (D) Lens epithelial cells arise from cells in the anterior of the lens vesicle proliferating, while primary fiber cells result from elongated cells of the posterior of the lens vesicle. (E) Lens epithelial cells (LECs) proliferate and differentiate into secondary fiber cells at the lens equator. (F) The lens continuously grows as fiber cells are continuously added on top of the older fiber cells. Lens fiber cells persist for the lifetime of a vertebrate. (Andley, 2008)

The mammalian lens is derived from the head surface ectoderm of the vertebrate embryo, and begins with the formation of the lens placode (Lang, 2004; Li and Piatigorsky, 2009), a thickened region of the head surface ectoderm that lies adjacent to the optic vesicle (Lang, 2004). The optic vesicle interacts with the surface ectoderm causing the lens placode to become the lens vesicle through coordinated invagination (Li and Piatigorsky, 2009; Lang, 2004). The anterior epithelium then proliferates to form the cuboidal epithelium along the anterior surface, and the posterior epithelial cells of the lens vesicle stop proliferating, exit the cell cycle, and begin to differentiate into the primary fiber cells (Lang, 2004; Li and Piatigorsky, 2009).

The epithelial cells overlying the lens vesicle become the corneal epithelium, and corneal stroma cells develop from the neural crest cells, which migrate under this cell layer. (Li and Piatigorsky, 2009). Many successive transcription factors, as well as multiple interactions and signaling pathways from certain growth factors are necessary for proper eye development (Li and Piatigorsky, 2009; Cvekl and Duncan, 2007), but the complete molecular mechanism is still elusive.

Function of the Mammalian Lens

The mammalian lens is responsible for the refraction of incident light, as well as focusing an image onto the retina (Land, 1988; Land and Fernald, 1992). The refractive power of the lens corresponds to a protein concentration gradient radiating from the center of the tissue (Piatigorsky, 2008), and the lens itself is avascular and non-innervated (Kuzak and Brown, 1994).

As mentioned, the lens is a relatively simple system that is composed of two distinct compartments, the epithelium and the lens fiber cell mass (Bhat, 2001). The organelle-free central region of the lens fiber cell mass provides the lens with its transparent phenotype, while the epithelium sustains this tissue metabolically, as well as providing a source of precursor cells that give rise to fiber cells (Piatigorsky, 1981; Bhat, 2001). The single-layer anterior lens epithelium that faces the cornea is composed of three areas of cells in the adult. The central epithelium contains mostly non-dividing cells, and is surrounded by the germinative zone, in which the cells are dividing. Below the germinative zone is the equatorial region, where the dividing cells differentiate into fiber cells. In total, the anterior epithelium ends at the conclusion of the anterior surface, or after the equatorial region (Bhat, 2001).

To comprehend lens development, a more complete description of lens fiber cell differentiation is necessary. In the beginning, the cells that line the lens vesicle have their apical surfaces pointing inwards and their basal surfaces outwards, contacting the basement membrane (the lens capsule) that encircles the vesicle. The development of the lens from the lens vesicle begins with the posterior epithelial cells differentiating into fiber cells, and in this process the cells elongate in an anterior-posterior manner, eliminating the lumen of the lens vesicle (Bhat, 2001). These are considered the primary fiber cells, and there now exists an apical interface, a contact between the elongated fiber cells and the apical surface of the anterior epithelial cells (Zamphigi et al., 2000). As a result of this process, the posterior portion of the lens no longer has epithelial cells and lens growth is now dependent entirely on the anterior epithelium (Bhat, 2001). After the formation of the primary fiber cells, lens fiber cell differentiation continues with the termination of cell division, and deliberate cell

elongation from progenitor cells at the lens equator forming the secondary lens fiber cells. Initiation of fiber cell development coincides with the expression of large amounts of the water-soluble crystallins. As the lens continues to grow, the fiber cells migrate further and further into the center of the lens, known as the lens nucleus. Here the cells will degrade all their organelles, lose contact with the epithelium and capsule at the apical and basal surfaces, respectively, form new contacts with adjacent fiber cells, and experience an increase in their lateral membrane folding (Piatigorsky, 2008; Beebe et al., 2001). Lens fiber cell differentiation continues to occur throughout an individual's entire lifetime, making concentric layers such that the newest fiber cells made from epithelial cells are added on top of older ones and the oldest fiber cells are at the deepest portion of the lens (Piatigorsky, 2008).

The lens is an ideal system to the modern biologist as there are no known recognizable cancers of this ocular tissue; it is an avascular, transparent system, and the anterior epithelium stays in a morphological state that allows for the study of the effects of aging on its function (Bhat, 2001). As a result, is often chosen as a structure to study development.

Cataracts and Posterior Capsule Opacification

Blindness and low vision, or bilateral vision worse than 20/40, affect approximately one in twenty-eight Americans over the age of forty years, and the number of blind people is projected to increase by 70% to 1.6 million people by 2020. Cataracts, the opacification or loss of lens transparency, is one of the leading causes of blindness worldwide, and is the leading cause of low vision in the United States (Congdon et al., 2004). Cataract has many causes, including DNA mutations, cell

damage and diabetes. During cataract surgery, or extracapsular lens extraction, the cloudy natural lens is removed from the eye in a way that maximizes removal of epithelial and fiber cells and reduces damage to the eye. The lens capsule is left behind to secure the implanted artificial intraocular lens. Unfortunately, all of the epithelial cells are often not entirely removed.

Posterior capsule opacification (PCO) is a condition that occurs when these remaining epithelial cells persist, proliferate, and migrate to the posterior portion of the lens in conjunction with the cells undergoing either epithelium-to-mesenchymal transition (EMT), a wound-healing process in which they evolve into mesenchymal cells, or aberrant fiber cell differentiation (Wormstone et al., 2009). The combination of epithelial cell growth and altered morphology can result in decreased effectiveness of the implanted intraocular lens – preventing lens accommodation - and may cause capsular wrinkling, all of which potentially result in decreased visual acuity overall, leading to what is clinically known as a “secondary cataract" (Spalton, 2011). PCO is the most common complication of cataract surgery, occurring in up to 50% of patients by two to three years after the operation. The treatment for PCO, Nd:YAG laser capsulotomy, is the third most common surgery performed on Medicare patients in the United States (Spalton, 2011; Steinberg et al., 1993). Ideally extracapsular lens extraction procedures would be performed in such a way that the damage to the lens epithelium would be minimalized and the eye would remain protected from wound healing responses such as PCO. This has not yet been achieved, however. In fact, PCO causes significant visual impairment in up to half of patients within 2 to 5 years of extracapsular cataract extraction, and rates of PCO occurrence increase thereafter (Clark, 2000). Researchers are currently investigating alternative shapes and materials

for the artificial intraocular lens implant that is used during cataract surgery, in addition to new surgical techniques, and hope to reduce the occurrence of PCO (Spalton, 2011).

Additionally, by studying cataracts and PCO, the factors that can stimulate or inhibit proliferation, migration, differentiation, and transdifferentiation of the lens epithelium can be identified. It is also known that, following surgery, the level of growth factors, and subsequent proteins, increases, and these modulators of cell function are stipulated to influence PCO development after cataract surgery (Wormstone et al., 2009). Transforming growth factor beta (TGFβ) has become the focus for those studying the biological basis of PCO. TGFβ is involved in cell proliferation, differentiation, migration, adhesion and apoptosis (Vandewalle et al., 2009). It has been found to regulate Smad signaling proteins in the nuclei of cells following cataract surgery, and TGFβ antibodies can suppress the wound healing process (Saika et al., 2001; Wormstone et al., 2009). Additionally, it has been proposed to serve as an immune regulator in the eye, and to potentially have a role in PCO, as there is now evidence that it is a powerful inducer of transdifferentiation of lens epithelial cells to mesenchymal cells (Hales et al, 1994; Wormstone et al., 2009). Researchers are currently working to optimize IOL materials and structure, develop more effective surgical techniques, with the overarching goal of significantly reducing the occurrence of PCO and improve the lives of millions (Wormstone et al., 2009).

The Role of SIP1

SMAD INTERACTING PROTEIN 1 (Sip1, also known as Zeb2, ZFHX1B, SMADIP1, FLJ42816, KIAA0569), a homeo-domain transcription factor of the two-handed E box binding zinc finger Zeb protein family (Comijn et al., 2001), is expressed during embryonic development of the eye in several tissues, including the lens and neural retina, and has been identified for its role in transcription regulation, functioning both as a repressor and activator of transcription activity. SIP1 has two clusters of zinc fingers, four at the N-terminus and three at the C-terminus, a homeodomain that participates mostly in protein-protein interactions, a Smad binding domain, and additional co-activator and co-repressor binding domains. It binds to members of the SMAD family of TGFβ signal transducing proteins, as well as directly to DNA, specifically to the consensus sequence 5'-CACCT(G). SIP1 shows preference in binding, such that it binds SMAD3 more often than SMAD2, and perhaps may contribute to the differing functions of SMADs *in vivo* through their regulation Grabitz, 2010).

Specifically in the eye, Sip1 expression is activated after lens placode induction (Higashi et al., 2005), and from a developmental view, lenses deficient in SIP11 from the lens placode stage fail to exhibit lens vesicle separation, are reduced in size and show delayed crystallin expression (Yoshimoto et al., 2005). Deletion of *Sip1* later in lens development results in cataractous lenses with abnormal fiber cell migration, although lens fiber cell marker expression is normal. Instead, loss of SIP1 from the lens vesicle stage results in inappropriate retention of early developmental marker gene expression in the mature lens (Manthey et al., submitted). In other epithelial tissues, SIP1 can repress epithelial gene expression, and activate

mesenchymal gene expression (Andersen et al., 2005; Vandewalle et al., 2005), making it essential for proper development and growth. Many important genes for the development and growth of the eye, especially E-cadherin, a cell adhesion molecule present in normal epithelial cells, have been reported to be target genes of SIP1 (Comijn et al., 2001; Vandewalle et al., 2009). Figure 2 (below, imaging done by Abby Manthey) shows that SIP1 begins to be highly expressed 10.5 days post conception (dpc), and that SIP1 is present in high levels beginning at the lens placode stage (lp) and continuing throughout adulthood in the epithelium (e) and the transition zone (tz), the place of fiber cell differentiation. By staining for SIP1 protein (red) and DRAQ 5/DNA (blue), it has been confirmed that SIP1 is expressing primarily in the lens cell nuclei, implicating a function as a nuclear transcription factor during lens development.

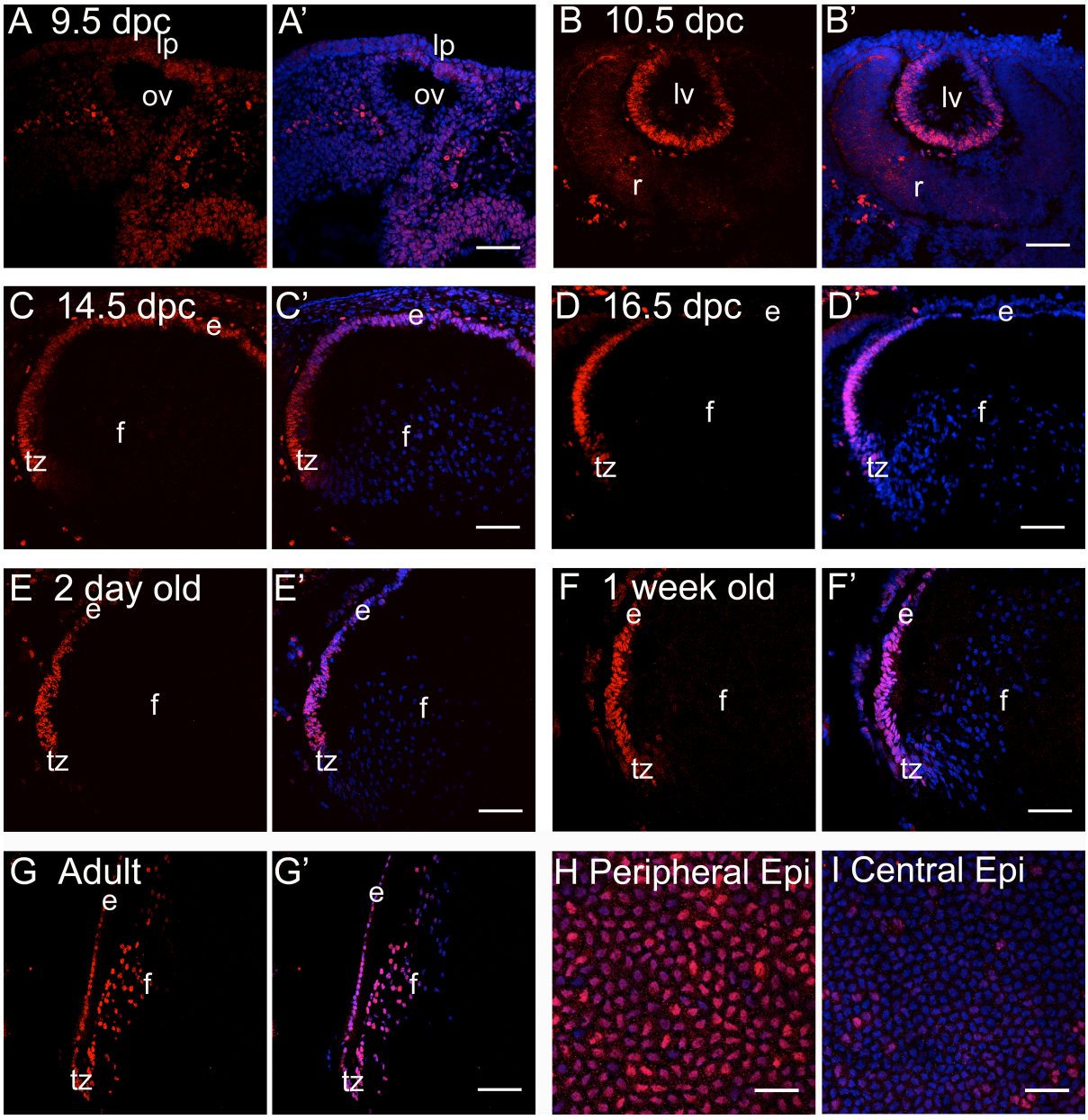
A 9.5 dpc
lp
ov
A'
lp
ov
B 10.5 dpc
lv
r
B'
lv
r
C 14.5 dpc
e
f
tz
C'
e
f
tz
D 16.5 dpc
e
f
tz
D'
e
f
tz
E 2 day old
e
f
tz
E'
e
f
tz
F 1 week old
e
f
tz
F'
e
f
tz
G Adult
e
f
tz
G'
e
f
tz
H Peripheral Epi
I Central Epi

Figure 2 Staining of SIP1 protein (red) and DNA (blue) from 9.5 dpc through adulthood in murine lens. A: SIP1 is present in the lens placode (lp) 9.5 dpc, and the optic vesicle (ov) is present. B: At 10.5 dpc, the lens vesicle (lv) is formed, and the retina (r) also has SIP1 expression. C-D: At 14.5 and 16.5 dpc, SIP1 is expressed throughout the epithelium (e) to the transition zone (tz), and it is not present in the fiber cells (f), which are nuclei-free. E: At 2 days old, SIP1 is still expressed in the epithelium and the transition zone, and is not seen in the fiber cells. F: At 1 week old, SIP1 is still present in the epithelium, and SIP1 is seen in a larger area of the transition zone, but less is expressed in the central epithelium. G: During adulthood, SIP1 is still seen in the epithelium, and transition zone, and its expression extends into the periphery of the fiber cell mass, but is mostly non-existent within the fiber cell area and the central epithelium. H-I: whole mount staining of the peripheral epithelium, and the central epithelium, respectively.

There has also been a recent focus on Sip1's role in the epithelial mesenchymal transition (EMT) during development and PCO, and in cancer progression (Vandewalle, 2009). Figure 3 (below, imaging done by Abby Manthey) shows that SIP1 protein is present in high levels during PCO both 48 hours and 5 days after cataract surgery. The expression profile seen at 48 hours is representative of robust PCO, a wound healing process, and this image confirms that it is highly likely that *Sip1* has a role in this pathway.

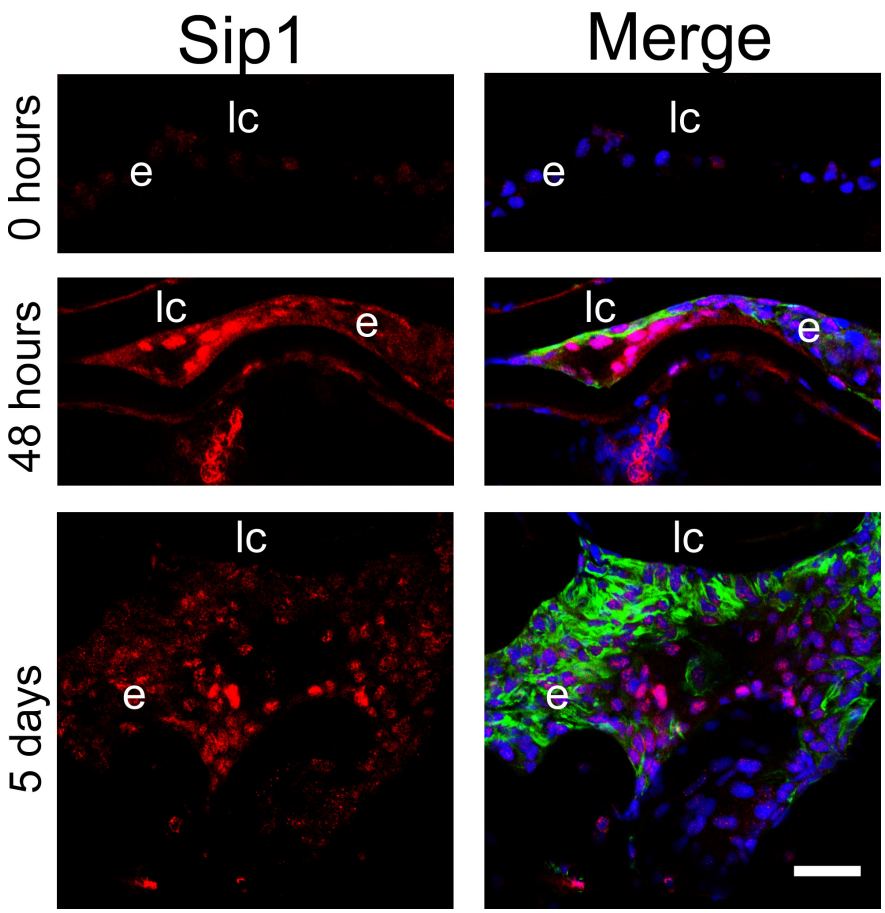

Figure 3 SIP1 protein (red), ALPHA-SMOOTH MUSCLE ACTIN (αSMA, green), and DNA (blue) staining 0 hours after surgery, 48 hours after surgery, and 5 days after surgery. SIP1 is highly expressed along with other classical PCO markers after surgery. Scale bar= 35 μm.

Additionally, Mowat-Wilson Syndrome in humans results from a heterozygous *Sip1* mutation, and is associated with Hirschsprung's disease (severe constipation), mental retardation, microcephaly, short stature, and a distinctive facial phenotype. A portion of these patients (14%) also presented with ocular deformities, including microphthalmia, cataract, iris coloboma and Axenfeld anomaly (Zweier et al., 2005). Increased levels of SIP1 PROTEIN have also been found in multiple types of cancer

such as breast, ovarian, gastric, pancreatic, and oral squamous cell carcinoma. Reports have also found ZEB proteins to be crucial in the development of cartilage, bone and muscle, and it has been shown that complete absence of SIP1 is incompatible with life after embryonic day 9.5 (Vandewalle et al., 2009). These findings place SIP1 in multiple developmental pathways, marking it as essential in the development of an organism as a whole (Vandewalle et al., 2009; Grabitz, 2010).

The Role of Alpha V Integrin

Integrins are transmembrane glycoprotein receptors that bind extracellular matrix proteins, cell surface immunoglobulin molecules, or other adhesion receptors on neighboring cells (Weis and Cheresh, 2011), as well as help organize the cytoskeleton (Tarone *et al*, 2000). Such interaction controls cell organization in organs and tissues throughout development as well as during cell differentiation and proliferation. It was hypothesized by many scientists that αV integrins would have crucial roles in cell growth, survival and migration, and would be critical in embryonic development. However, even though they experience intracranial and/or gastrointestinal hemorrhaging causing them to die during embryonic development or soon after birth, mice lacking the αV subunit develop almost completely normally, suggesting that the αV integrin subunit is not necessary for development and cellular differentiation, with the small exception of a few blood vessels (Sheppard, 2004). However, additional studies have shown that αV integrins have highly specialized roles. J.P. Thiery and coworkers gave one of the first examples of the importance of integrins in development when they showed how neural crest cells use integrins to

move along the fibronectin rich matrix to reach their final destination in the embryo (Tarone *et al*, 2000).

The term integrin refers to their ability to functionally integrate the extracellular matrix with the cytoskeleton across the plasma membrane (Tarone *et al*, 2000). Binding specificity is possible because of the noncovalent heterodimeric pairing of one α and one β subunit (Weis and Cheresh, 2011). There are 17 α and 8 β subunits that are expressed in over 20 different combinations on cell surfaces (Mousa, 2003). Both subunits are required to make the ligand-binding pocket, but as heterodimers sharing a common β subunit with distinct α subunits bind different ligands, the α subunit is likely to have a more dominant role in determining binding selectivity. Ligand binding at the cell surface requires a divalent cation, and at the cytoplasmic face of the plasma membrane integrins bind to cytoskeletal proteins of the actin contractile system (Tarone *et al*, 2000). Inactive integrins are usually found scattered throughout the cell surface, but upon activation by binding to the ECM, they cluster into focal adhesion complexes, which may instigate integrin signaling (Mamuya and Duncan, 2012).

αV integrin subunit in particular can bind with β1, β3, β5, β6, and β8 subunits, forming a subfamily of five members, and especially recognizes the canonical tripeptide recognition sequence, arginine-glycine-aspartic acid (RGD), (Sheppard, 2004) on certain matrix protein ligands such as fibronectin, vitronectin, collagens, and thrombospondin. Many integrins act as positional receptors to generate intracellular signals to control cell survival and proliferation (Tarone *et al*, 2000). Different integrin pairs recognize different ligands, and some pairs can recognize several ligands. For example, αVβ5 integrin preferentially binds vitronectin and fibronectin.

The integrins present on the surface of the cell determine its adhesion, motility, cell signaling and survival capabilities in a particular environment, and the αV integrins are especially important during tissue remodeling in wound repair, angiogenesis, and cancer. Interestingly, αV integrin subunit KO mice fail to exhibit PCO, consistent with the fact that PCO is a mixed differentiation and wound healing process and αV integrin subunit is involved in these processes (Mamuya et al, manuscript in preparation). In the WT mouse, however, αV integrin protein levels increase during PCO. This is shown below in Figure 4.

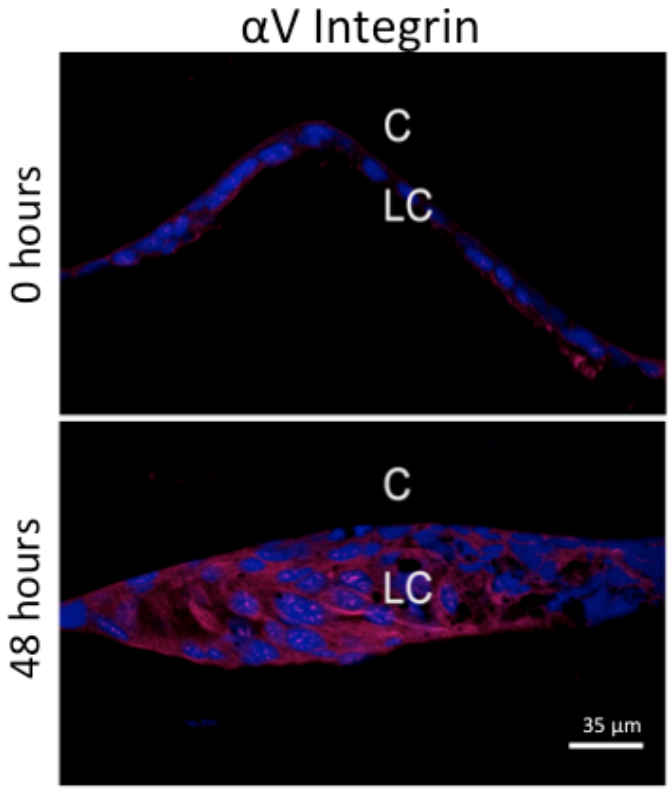

Figure 4 αV integrin levels upregulate at 48 hours post-surgery (during PCO). C is the cornea, and LC are the lens cells. Blue is DNA, and red is αV integrin. Scale bar= 35µm.

Another example of integrin involvement occurs in tumor cells, which change their integrin expression profiles to enhance their ability to migrate, invade, metastasize, and survive in new environments (Weis and Cheresh, 2011). Integrin-ligand interaction inhibition suppresses cellular growth and induces apoptotic cell death (Mousa, 2003). In other words, integrin cell matrix adhesion prevents apoptosis, providing a control mechanism in tissue formation and homeostasis to eliminate cells that are in an improper location (Tarone *et al*, 2000).

Additionally, integrins bind directly to a number of growth factors including TGFβ, whereby stimulating growth factor signaling upon their interaction (Weis and Cheresh, 2011). There is also a circle of regulation present between integrins and TGFβ. As many αV integrins are upregulated during EMT, the TGFβ signaling that induces EMT is likely to have a critical role in the upregulation of integrin expression. One recent study showed that TGFβ signaling induced surface expression of αVβ3 integrin in human lung fibroblasts via a β3 integrin subunit, c-Src-, and p38 MAPK-dependent pathway. Alternatively, TGFβ can indirectly induce integrin expression through upregulation of ECM protein expression, which in turn stimulates integrin expression. Furthermore, many αV integrins contain a RGD sequence that interacts with the latent form of TGFβ (the form that it is secreted in) upon which the growth factor is activated and can initiate receptor-mediated signaling. There are two proposed models for the activation mechanism of TGF, both of which appear to be cell specific. However, it still remains unclear why TGFβ signaling pathways and activation mechanisms are tissue and cell specific, and little is known about how one process affects the other (Mamuya and Duncan, 2012).

As mentioned previously, TGFβ signaling regulates EMT. However, this signaling is not a direct linear process, but rather it proceeds by sequentially inducing a complex network of signaling cascades that crosstalk with other pathways, with the cumulative effect of successfully inducing EMT. Cross-talk between TGFβ and integrins can occur downstream of the initial receptor activation through interwoven MAPK, P13K, RAS/RHO and small GTPase pathways, or even via TGFβ-induced phosphorylation of integrins, and integrin-induced receptor tyrosine kinase activation leading to activated TGFβ. There are many possible instances of cross-talk between TGFβ and integrins, many of which initiate TGFβ signaling to stimulate MAPKs, initiating EMT and invasion in epithelial cells (Mamuya and Duncan, 2012). All in all, integrins and TGFβ signaling pathways are highly interwoven, and both may induce expression of the other through a circle of feed-forward cross regulation, which ultimately leads to EMT.

Furthermore, Fahmy Mamuya showed that *αV integrin* mRNA levels decrease during PCO with a -4.33 ±1.08 fold change at 24 hours post-surgery even though αV integrin protein expression levels increase. This is shown below in Figure 5 (Mamuya et al, manuscript in preparation).

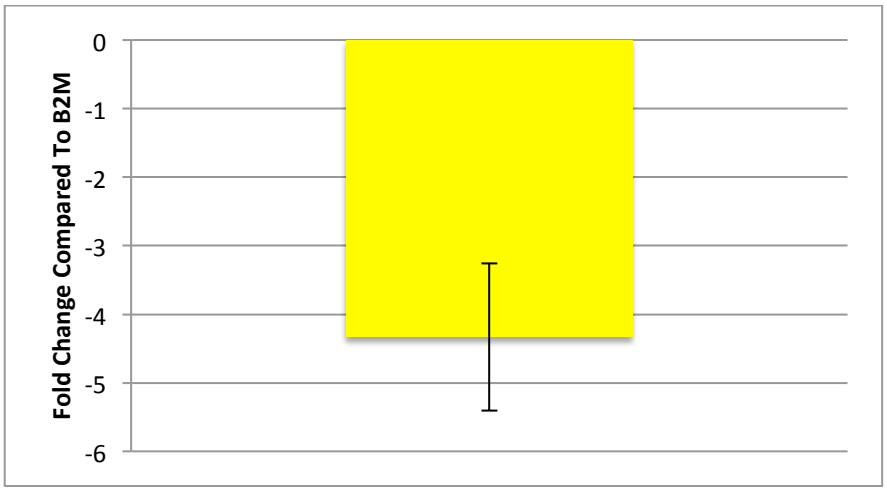

Figure 5 The *αV integrin* mRNA levels have a fold change of -4.33 ± 1.08 at 24 hours post-surgery, showing that the RNA levels do not increase relative to protein levels. $p < 0.001$

It is quite plausible that PCO is not under transcriptional control, but rather by a post-transcriptional mechanism, and it is possible that microRNAs (described below) are involved.

miRNAs: Definition and Role in the Lens

Recently, regulation of *Sip1* function by microRNAs has taken center stage in the control of both development and abnormal cellular changes. MicroRNAs (miRNAs) are small, non-coding RNA sequences of ~22 nucleotides that bind to complementary sequences in the 3' UTR of messenger RNA (mRNA), specifying translational repression through sufficient complementarity, directing site-specific degradation with extensive complementarity of their mRNA targets, signaling transcriptional silencing, and participating in RNA interference (RNAi). They may

further repress translation by slowing or stalling the ribosomes, or by degrading the newly synthesized polypeptide, rendering translation nonproductive. It has also been noted that the miRNA pathways of plants and animals appear to be biochemically indistinguishable from the posttranscriptional gene-silencing pathway, a RNA silencing pathway, in those same species (Bartel, 2004). It has been estimated that one-third of all human mRNAs are regulated by miRNAs (Augoff *et al*, 2011). On a more macro-level, they can control cell death, cell proliferation, fat metabolism in flies, neuronal patterning in nematodes, modulation of hematopoietic lineage differentiation in mammals, and leaf and flower development in plants (Bartel, 2004). In essence, miRNAs are gene regulatory switches, and are key regulators of biological processes (Bartel, 2004; Karali et al., 2010).

It has been determined that miRNAs usually derive from independent transcriptional units, but they can be processed from the introns of pre-mRNAs as well. There is also evidence of miRNA gene clustering. Many miRNAs have unique expression patterns, and, more specifically, they are expressed differentially during specific stages of development (Bartel, 2004). One miRNA can affect a broad network of genes, and most are essential to normal cell activity. This leads to the possibility of being able to "micromanage" the transcriptome (Bartel, 2004). Defects in miRNA function have profound effects on development (Karali et al., 2010). Their complex, highly relevant gene regulatory functions render it important to discover all genomic miRNAs so as to better understand molecular pathways such as cellular differentiation (Hansen et al., 2010).

One study done by Gregory *et al*. showed that five members of the miR-200 family, miR-200a, miR-200b, miR-200c, miR-141 and miR-429, as well as miR-205,

are downregulated in cells undergoing EMT. Levels decreased with subsequent exposure to TGFβ, and also were observed simultaneously with an *E-cadherin* mRNA decrease, and increases in δEF1, SIP1, fibronectin and N-cadherin proteins, all of which are mesenchymal markers. The group also found that downregulation of these miRNAs is an essential component of EMT (Gregory *et al*, 2008).

To be more specific, it has been shown that miR-200c and miR-200b repress endogenous protein expression of *Sip1* and *δEF1*. Using a target prediction computer program, *Sip1* mRNA was predicted to contain multiple binding sites for miR-200b, and miR-200c and miR-429, as they contain the same binding sequence, and indeed, its behavior changed with miR-200b manipulation. Similarly, miR-200a, and subsequently miR-141, were also predicted to have multiple binding sites. It was shown that each of these miRNAs represses *Sip1* expression and act in an additive manner, confirming the idea that *Sip1* is a key miRNA target. The loss of miR-200b alone induced SIP1 protein expression, which was amplified upon subsequent inhibition of miR-200a and miR-205, and this was sufficient to induce EMT. Additionally, EMT coincided with an upregulation of SIP1, showing that control of *Sip1* by the miR-200 family and miR-205 is critical for the EMT process. Upon expression of these miRNAs, SIP1 protein levels were reduced and a mesenchymal epithelial transition (MET)-like process ensued in the cells, demonstrating the reversibility of the EMT process (Gregory *et al*, 2008).

Furthermore, it was observed that the presence of miR-200 family miRNAs corresponded to an epithelial phenotype, and that *Sip1* (and *δEF1*) mRNA levels were strongly inversely correlated with miRNA-200 family expression (Park *et al,* 2008; Gregory *et al*, 2008). These studies were performed in multiple cell types with similar

findings, and it has been proposed that the miR-200 family may facilitate the degradation of *Sip1* mRNA, in addition to inhibiting its translation (Gregory *et al*, 2008). Finally, miR-200b, miR-200a, and miR-429 are coordinately repressed by SIP1 (and δEF1) protein, indicating that the miR-200 family may be regulated by *Sip1*, and presenting the idea of the existence of a reversible double negative feedback loop between the miR-200 family and the ZEB proteins (Figure 6) that regulates EMT and cell phenotype (Bracken *et al,* 2008; Gregory *et al*, 2008).

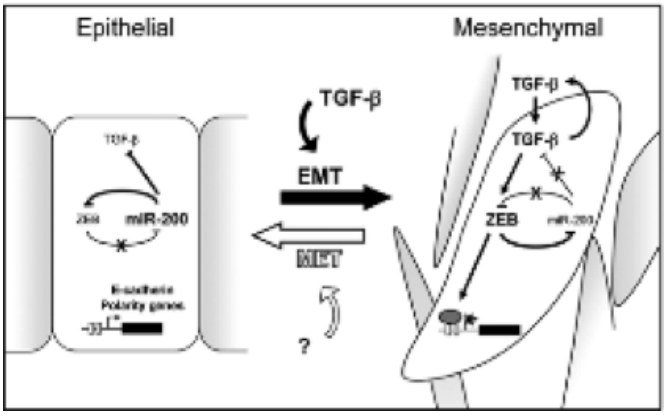

Figure 6 The double-negative feedback loop between the miR-200 family and ZEB proteins (Gregory et al., 2008).

During oncogenesis for example, the reversible nature of the double feedback loop makes it possible for cells that have undergone EMT and escaped the primary tumor, to return to the epithelial state at an alternative site to form a secondary tumor (Gregory *et al*, 2008). As shown above, SIP1 protein is seen in high levels during the development of the normal lens, as well as during the wound healing process after

cataracts surgery, leading to the hypothesis that the miR-200 family controls *Sip1* expression.

However, Karali *et al* performed a microRNA expression atlas of the mouse eye detailing relative expression levels of 285 miRNAs. Their study noted that miR200 family members are expressed at low levels in the lens while miR31 was present in high levels in both the lens and corneal tissue. Interestingly, another recent study identified and characterized miR31 as a master regulator of integrin expression because of its capacity to directly target seed sequences in the 3'UTR of the *αV integrin subunit* mRNA, in addition to those of *α2, α5* and *β3 subunits*, leading to their posttranscriptional repression. Repression of these alpha subunits led to subsequent repression of the β1 subunit. As integrins are essential for cell adhesion and spreading by mediating cell-matrix interactions, miR31 expression can have profound effects during development, cancer, and the wound healing response and as a result is considered a master regulator (Augoff *et al*, 2011). Since similar processes occur during PCO, it is thus plausible that miR31 is involved in the condition.

Only one snap shot of the miRNAs present in the eye has been previously studied. This study identified 39 unique miRNAs in the lens alone, and suggested that the development, maintenance and function of the eye accompany the expression of a wide set of miRNAs, which portray a coordinated and distinct expression pattern among the various tissues of the eye (Karali et al., 2010). Studying the temporal and spatial expression patterns of the miRNAs of the lens will not only support the hypothesis that the miR-200 family controls the function of *Sip1*, but it will also help to elucidate the targets, modifiers and pathway of *Sip1* in EMT, and could support the

idea that miR31 is involved in integrin control and PCO. This will help to determine the molecular basis of eye development, as well as eye disease.

Chapter 2

METHODS

Creating the Sip1 Expression Vector

Polymerase Chain Reaction (PCR)

PCR was first performed on the original *Sip1* fragment with primers from IDT and PrimeStar Polymerase Master Mix to amplify and isolate the fragment from the pCMV plasmid. The primer sequences used were:

Forward:

5'- ACA GGC CTT GGC GCG CCT AAG CAG CCG ATC ATG GCG GAT

Reverse:

5'- TGC TCG AGT GCG GCC GCC TGC AGT AGT TTA TTA CAT GCC

An Eppendorf Mastercycler was used to complete thirty cycles of 15 seconds at 94°C, 5 seconds at 58°C and five seconds at 72°C. The sample was then run on a 1% agarose gel for 70 minutes at 120 volts, and purified using Promega's Wizard® SV Gel and PCR Clean-Up System. The Nanodrop was then used to determine concentration.

PCR was performed a second time with a reaction mixture of 0.714µL purified *Sip1* fragment, 25µL Primestar HS Mix, 1µL of each forward and reverse Takara primers, and 22.29µL nuclease-free water. The same PCR cycles were used as

above, and, again, the sample was run on a 1% agarose gel at 120 volts, extracted and purified. The concentration was determined via Nanodrop.

Cloning

Blunting Kination Reaction:

This reaction was necessary because the *Sip1* PCR product was cloned into a blunt-end vector, and the extra base pairs at the 3' end and the phosphate at the 5' end must be removed to properly integrate it during the ligation reaction. In order to provide the restriction enzymes used below with enough cDNA to reliably cut on either side of the *Sip1* fragment, the PCR product obtained above was used in a Takara Mighty Cloning Kit (Blunt End) kit that will ultimately produce an intermediate plasmid containing the *Sip1* cDNA fragment. A blunting kination reaction mixture of 2µL PCR product, 2µL 10X Blunting Kination Buffer, 1µL Blunting Kination Enzyme Mix, and 15µL distilled water was incubated at 37°C for 10 minutes. Then, 80µL distilled water and 100µlL phenol/chloroform/isoamyl alcohol (25:24:1) were added and the reaction mixture was centrifuged at 12,000rmp for 5 minutes. The supernatant was removed, and mixed with an equal amount of chloroform/isoamyl alcohol (24:1). Again it was centrifuged. The supernatant was then mixed with 10µL 3M sodium acetate and 250µL chilled ethanol, and kept at -80°C for 20 minutes. It was then centrifuged at 12,000rpm for 10 minutes at 4°C. The precipitate was washed with 70% ethanol, and then centrifuged at 12,000rpm for 5 minutes at 4°C. The precipitate was dried and dissolved in 20µL Qiagen® TE Buffer.

Ligation Reaction:

5µL of the DNA solution obtained above was mixed with 1µL pUC118 *Hinc* II/BAP and 6µL Ligation Mighty Mix, and then incubated at 16°C for 1 hour.

Transformation:

One Shot® TOP10 Chemically Competent *E. coli* cells were used with 100µg/mL ampicillin-50µg/mL X-gal LB agar plates. An ampicillin rapid transformation procedure was followed. 6µL of the ligation mixture were added to a thawed 50µL vial of One Shot® cells. The vial was incubated on ice for 5 minutes, and then heat-shocked for 30 seconds at 42°C, before being placed on ice again for 2 minutes. 50µL of transformed cells were spread across a pre-warmed plate using sterile technique, and the plate was incubated overnight at 37°C. Cultures were made from the white colonies, and a Promega PureYield™ Plasmid Miniprep System kit was used to purify the DNA. The Nanodrop again was used to determine final concentration.

Digestion

Digestion of the intermediate *Takara-Sip1* product was performed with the restriction enzymes AscI and NotI-HF. A mixture of 19.9µL *Takara-Sip1* product, 3µL NEB NotI-HF, 5µL NEB AscI, 0.5µL NEB BSA, 5µL 10X NEB Buffer 4, and 16.6µL nuclease-free water were combined, and the mixture incubated overnight at 37°C. The digestion reaction was run on a 1% agarose gel, and purified as above. The band for *Sip1* was observed at ~3600 base pairs.

Similarly, a digestion was performed on the pET-41a empty vector that Abby Manthey had prepared previously. A mixture of 4.484µL pET-41a vector, 3µL NEB NotI-HF, 5µL NEB AscI, 0.5µL NEB BSA, 5µL 10X NEB Buffer 4, and

32.02µL nuclease-free water were combined, and incubated overnight. Electrophoresis on a 0.9% agarose gel at 100 volts for 109 minutes was performed. A band at ~5900 base pairs was observed and excised. The band was purified using a Promega Wizard® SV Gel and PCR Clean-Up System, and the Nanodrop was used to determine concentration.

Ligation

A ligation reaction of 7.8µL *Sip1* fragment, 1.9µL pET-41a (+) fragment, 2µL NEB T4 DNA ligase, 2µL NEB 10X Ligase Buffer, and 6.3µL nuclease-free water was incubated overnight at room temperature.

Transformation

A transformation of the ligation mixture was performed using Invitrogen One Shot® TOP10 Chemically Competent *E. coli* cells (as above) with 100µg/mL kanamycin plates. 3µL of the ligation mixture was added to a 50µL vial of One Shot® cells, which was then incubated on ice for 30 minutes before being heat-shocked at 42°C for 30 seconds. The vial was then placed on ice for 2 minutes, and 250µL of Invitrogen S.O.C. Medium was added using sterile technique. This was then shaken at 37°C for 1 hour at 300rpm. 100µL of this mixture were spread over a pre-warmed kanamycin LB agar plate, which was incubated at 37°C overnight. These colonies were then screened using Promega PureYield Plasmid Miniprep System and agarose gel electrophoresis. The appropriate sample was sent for sequencing to firm that a Sip1 expression vector had indeed been made.

IPTG-induced Protein Expression

Protein synthesis occurred in biological material shaken at 300rpm at 37°C. FischerBiotech's IPTG, a synthetic analog of lactose, was added during translation to inactivate the lac repressors in the *Sip1* cDNA, thus activating the genes of the T7-lac operon promoter, which is responsible for lactose metabolism and regulation, and inducing protein synthesis. The target gene, *Sip1*, replaces the lac operon's natural lacZ gene, and translation of the target gene begins as the lac operon is activated. In addition, the cell cannot break down the IPTG, as it does lactose, and the pathway remains turned on, meaning that SIP1 protein will be expressed continuously under ideal conditions. Aliquots of the induced media were taken at regular intervals, and protein synthesis was monitored via SDS-PAGE.

SDS-PAGE

Before running the SDS-PAGE, a 100µL aliquot of a mixture of 95% BIO-RAD Laemmli Sample Buffer and 5% β-mercaptoethanol was added to 1mL of protein aliquot (as described above). The samples were boiled for five minutes. Samples were loaded into BIO-RAD Mini-PROTEAN® TGX™ precast gels, and run for 65-85 minutes at 100 volts. The gel was dyed with Invitrogen™ SimplyBlue™ SafeStain for 2 hours while being shaken gently at room temperature. It was then washed with deionized water for 2 hours, and then again for 1 hour. Gels were photographed using Coomassie® white light-white background conditions with a Carestream Gel Logic 212Pro Molecular Imaging System. This will determine if SIP1 is indeed being expressed, and if it is being expressed in high yield.

TaqMan® Small Assay qRT-PCR

Abby Manthey, a graduate student of the Duncan lab, had previously isolated the total RNA from the fiber or epithelial cells of her Sip1 KO and WT mice. I then used the Nanodrop to quantify the amount of RNA in each sample, as the concentrations varied among the samples. Taqman® miRNA and snoRNA primers compatible with Taqman® Small RNA Assays from Life Technologies™ that were known to occur in the eye, act as a control or interact with *Sip1* were used. Reverse transcription was performed in an Eppendorf MasterCycler using a TaqMan® microRNA Reverse Transcription kit to make cDNA. Each reaction contained 0.15µL 100mM dNTPs, 1.00µL MultiScribe Reverse Transcriptase, 1.50µL 10X Reverse Transcription Buffer, 0.19µL RNase Inhibitor, 4.16µL nuclease-free water, 5µL total RNA and 3µLTaqMan® Small RNA Assay (5X). Originally I started with 1ng of total RNA for each reaction, but this was insufficient, and I obtained better results upon using 20ng per reaction. Quantitative real-time PCR was then performed with an ABI Prism 7300 Sequence Detection System. A TaqMan® Small RNA Assay protocol was followed and the reactions occurred in a MicroAmp® Optical 96-Well Reaction Plate. Each well contained 1.33µL of cDNA, 7.67µL of nuclease-free water, 10.00µL TaqMan® Universal PCR Master Mix II (no UNG), and 1.00µL TaqMan® Small RNA Assay (20X). Each cycle of the qRT-PCR run should double the amount of double-stranded DNA, which is observed through an increase in fluorescence. The data output is in the form of C_T, the PCR cycle at which a fluorescence threshold was reached, and analysis is done to normalize the sample C_T values and to obtain the expression ratio between the sample and the control gene, which should remain consistent throughout all samples.

RNA Isolation

Dr. Yan Wang, a member of the Duncan lab, had previously surgically removed complete 0hr post-surgery and 24hr post-surgery WT and KO lenses from their respective mice. Using Promega's SV Total RNA Isolation System, total RNA was isolated from these samples. 175µL of RNA Lysis Buffer (with BME added) was added to the tube containing the lens tissue sample. The tissue was homogenized until no visible tissue fragments remained. Then 350µL of RNA Dilution Buffer was added to 175µL of lysate, and the tube was inverted four times to mix it. Next, the tube was placed in a water bath at 70°C for 3 minutes. After, the sample was centrifuged for 10 minutes at 13,000 x *g*. The cleared lysate solution was transferred to a clean microcentrifuge tube by pipetting, upon which 200µL of 95% ethanol was added. This solution was mixed by pipetting 4 times. Then the mixture was transferred to the Spin Column Assembly, and centrifuged for one minute at 13,000 x *g*. The flow-through liquid was discarded and 600µL of RNA Wash Solution (previously diluted with ethanol) to the Spin Column Assembly. It was then centrifuged for one minute at 13,000 x *g*. Next, 50µL of DNase incubation mix (40µL Yellow Core Buffer, 5µL 0.09M $MnCl_2$, and 5µL of DNase I enzyme per sample mixed by pipetting) was added directly to the membrane inside each spin basket. This was then incubated at 20-25°C for 15 minutes, after which 200µL of DNase Stop Solution (with added ethanol) was added. It was centrifuged at 13,000 x *g* for one minute before 600µL of RNA Wash Solution (with ethaol added) was added. Centrifugation was repeated. The flow-through was discarded, 250µL RNA Wash Solution was added, and the assembly was centrifuged at high speed for two minutes. The Spin Basket was transferred from the Collection Tube to the Elution Tube, and 50µL Nuclease-Free Water was

added. This was centrifuged at 13,000 x g for one minute. The concentrations of the purified RNA samples were determined with the Nanodrop, and then they were stored at -80°C.

cDNA Synthesis

The RNA samples previously isolated were used to create cDNA with SA Biosciences RT^2 RNA QC PCR Arrays Kit. First the RNA samples were diluted to a total volume of 8µL of 128ng/µL RNA in total. To each RNA diluted sample, 2µL of Genomic DNA Elimination Mixture (GE 5X gDNA Elimination Buffer) were added, and the contents were mixed gently with a pipette. Then the samples were centrifuged briefly, and incubated for 5 minutes at 42°C. After, they were chilled immediately on ice for at least one minute. In the meantime, a reverse transcription cocktail was made consisting of 4µL BC3 (5X RT Buffer 3), 1µL P2 (primer and external control mix), 2µL RE3 (RT Enzyme Mix 3), and 3µL RNase-free water for each reaction. Enough was made for 5 reactions. The last component in cDNA synthesis was the first strand cDNA synthesis reaction. For this, 10µL of RT cocktail were added to each genomic DNA elimination mixture, which were mixed gently with a pipette. These were incubated at 42°C for exactly 15 minutes and then heated at 95°C for 5 minutes to stop the reaction. Finally, 91µL of double distilled water were added to each 20µL of the cDNA synthesis reaction and mixed well. These were stored at -20°C.

SYBR Green qRT-PCR

The cDNA samples synthesized from the isolated RNA as previously described were used with an ABI Prism 7300 Sequence Detection System to perform

qRT-PCR. 96-well plates were used for each run, and triplicate technical replicates were performed for each reaction, which consisted of 2µL cDNA, 12.5µL SYBR green, 1µL of 1X forward primer (previously diluted from 10X), 1µL of 1X reverse primer (previously diluted from 10X), and 9.5µL of nuclease-free water. Primers were created for vitronectin, tenascin C, fibronectin and α-smooth muscle actin cDNA by graduate student Fahmy Mamuya, and *B2M* was used as a housekeeping gene. As mentioned above, each cycle of the qRT-PCR run should double the amount of double-stranded DNA, which is observed through an increase in fluorescence. Data analysis is performed in the same manner as described previously.

Statistical Analysis

Statistical analysis was performed using nested ANOVA after relative fold changes were determined. In order to do so the data were first normalized by log transformed each value (fold change). Nested ANOVA was performed because the positive and negative variances were different. There were two null hypotheses: 1) the Ct values for each miRNA have the same mean (within group), and 2) all miRNA Ct values have the same mean (between groups). Calculations were performed in Microsoft Excel, with the aid of graduate student, Anne Terrell.

Chapter 3

SPECIFIC AIM 1: USE *ESCHERICHIA COLI* TO PRODUCE AN ANTI-SIP1 ANTIBODY

Full length SIP1 protein is unavailable commercially. The Sip1 antibody currently used in the lab is unreliable and requires a tedious protocol for immunstaining while it is ineffective for chromatin immunoprecipitation. In order to facilitate *Sip1* studies, my first aim was to produce recombinant SIP1 protein suitable to produce an anti-Sip1 antibody by creating an expression vector and then using *E. coli* for expression of SIP1 protein.

I successfully produced and sequenced a prokaryotic expression vector, consisting of GST-tagged Sip1 cDNA cloned into the pET-41(α) vector. A map of the expression vector is given below in Figure 7. Specifically important features of the construct include the *Sip1* gene insert, Kanamycin resistance gene (allowing the vector to be selectively grown in media), the His-tag and GST-tag genes (important for protein isolation and purification), the Not1 and Asc1 restriction enzyme cut sites, and the T7 lac operon promoter (responsible for lactose metabolism and regulation).

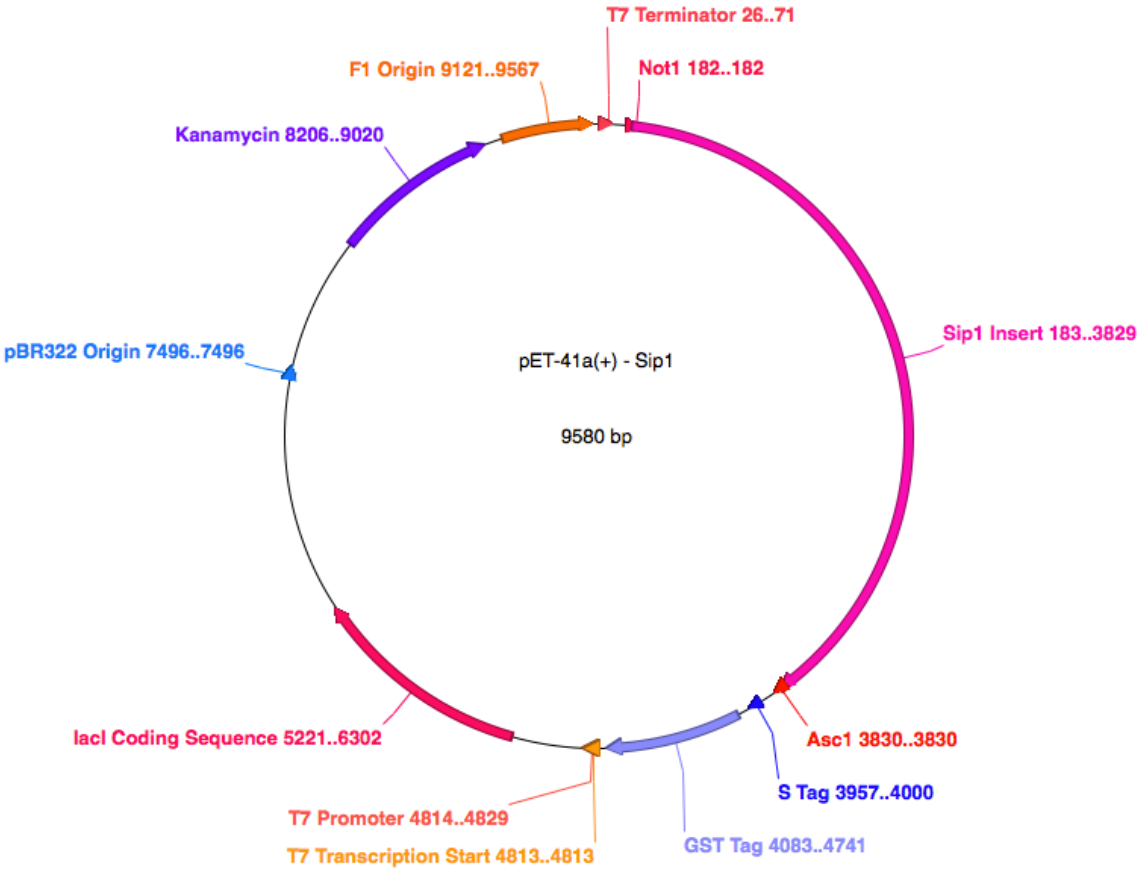

Figure 7 Sip1-pET-41a (+) expression vector map.

Digestion techniques were performed with the restriction enzymes NotI-HF (High Fidelity™) and AcsI. Images of the digested pET-41α vector and *Sip1* insert after agarose gel electrophoresis are shown below (*Figures 8 and 9,* respectively).

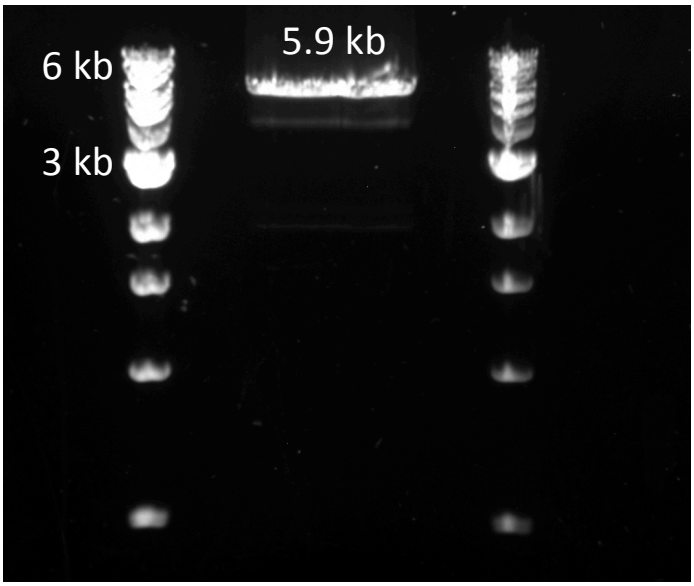

Figure 8 Agarose electrophoresis of the pET-41α empty vector after digestion, with a band at ~5900 base pairs (bp). There is also a small portion of undigested vector remaining.

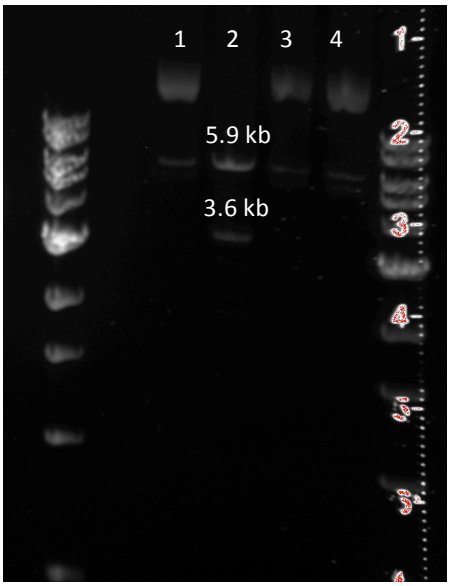

Figure 9 Agarose electrophoresis of several samples of the expression vector. The sample (column 2) with bands at ~3600 base pairs (*Sip1* insert) and ~5900 base pairs (pET-41α vector) was the correct expression vector.

The expression vector was sequenced by the University of Delaware's DNA Sequencing & Genotyping Center at the Delaware Biotechnology Institute. It was determined that *Sip1* and *GST* are in frame, and that *Sip1* is in the expression vector. The preliminary sequencing diagrams of the expression vector made in Sequencher 5.0 showing the *Sip1* insert and the pET-41α vector are presented below (*Figures 10 and 11*).

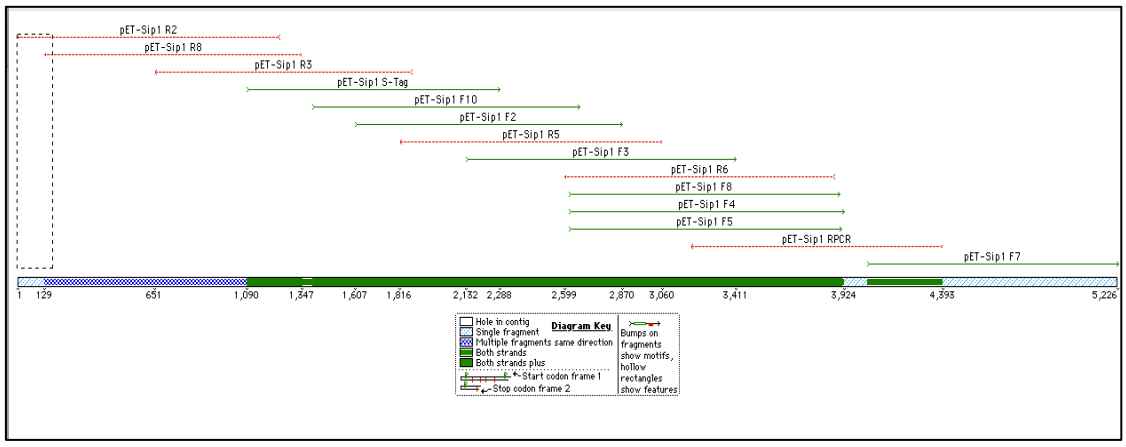

Figure 10 *Sip1* insert component of the expression vector

Figure 11 pET-vector component of the expression vector

I then used the synthesized recombinant *Sip1* DNA in protein expression experiments. I originally incubated the competent cells for six hours before inducing SIP1 protein production with isopropyl-β-D-thio-galactoside (IPTG). IPTG, a synthetic analog of lactose, will inactivate the lac repressors in the *Sip1* cDNA, thus activating the genes of the T7-lac operon promoter, which is responsible for lactose metabolism and regulation ("IPTG," 2012). The target gene, *Sip1*, replaces the lac operon's natural *lacZ* gene, and translation of the target gene begins as the lac operon is activated. In addition, the cell cannot break down the IPTG, as it does lactose, and the pathway remains turned on. For a control, I used the same protocol on a sample of the empty pET-vector (without the *Sip1* insert) to show normal protein expression patterns. I monitored the protein synthesis reaction every hour for four hours after induction, and performed SDS-PAGE analysis. These results are given below (*Figures 9 and 10*). Specifically, Figure 12 shows the absence of SIP1 protein at its expected 136 kD, and Figure 13 shows no protein expression at all.

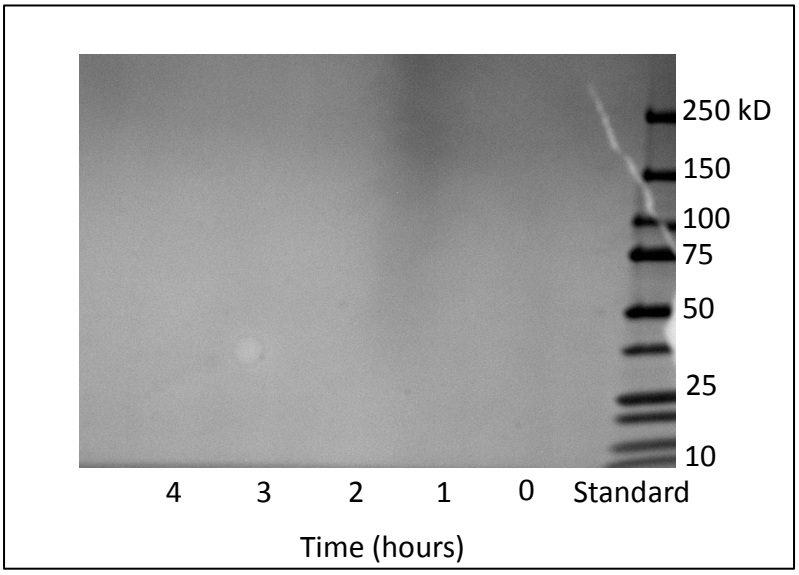

Figure 12 SDS-PAGE of the pET-41α empty vector. The right-most column is the Precision Plus Protein™ Standards Dual Color, and from right to left, the four columns protein samples are taken after 1 hour, 2 hours, 3 hours, and 4 hours after induction, respectively. There was no protein expression seen in the sample taken before induction either.

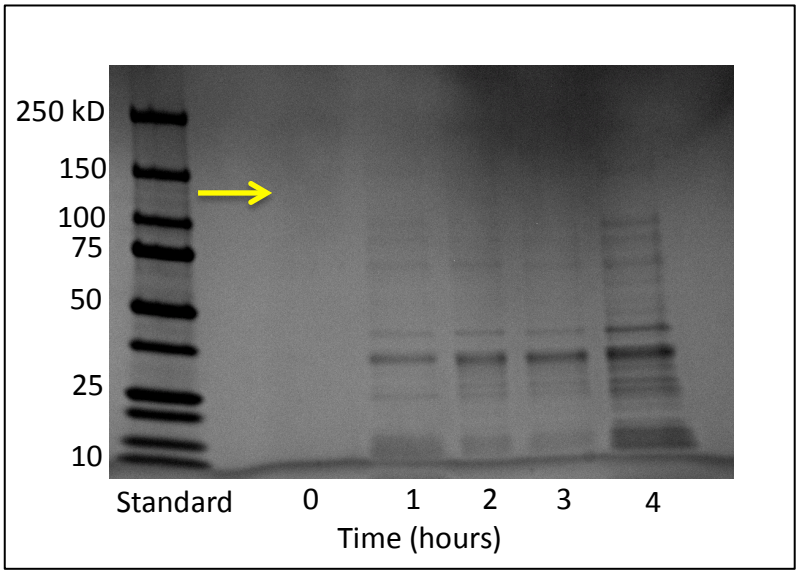

Figure 13 SDS-PAGE of the pET-41α vector with the *Sip1* insert. The column on the far left is the Standards Dual Color. The yellow arrow indicates 136 kD, the size of SIP1 protein. The band representing SIP1 (at 136kD) was expected to both be present, and darken significantly more than the other bands in relation because it was specifically induced. However, there is no such protein gradient.

Since there should have been protein expression for both samples, and darkening protein gradient as time increased after induction, I performed the experiments again over the course of a longer time period. This time, I incubated the competent cells for 8 hours before inducing protein synthesis and stopping cell synthesis. I then monitored the protein synthesis for the next 25 hours, taking samples every four hours. The SDS-PAGE images from these experiments are given below (*Figures 14 and 15*).

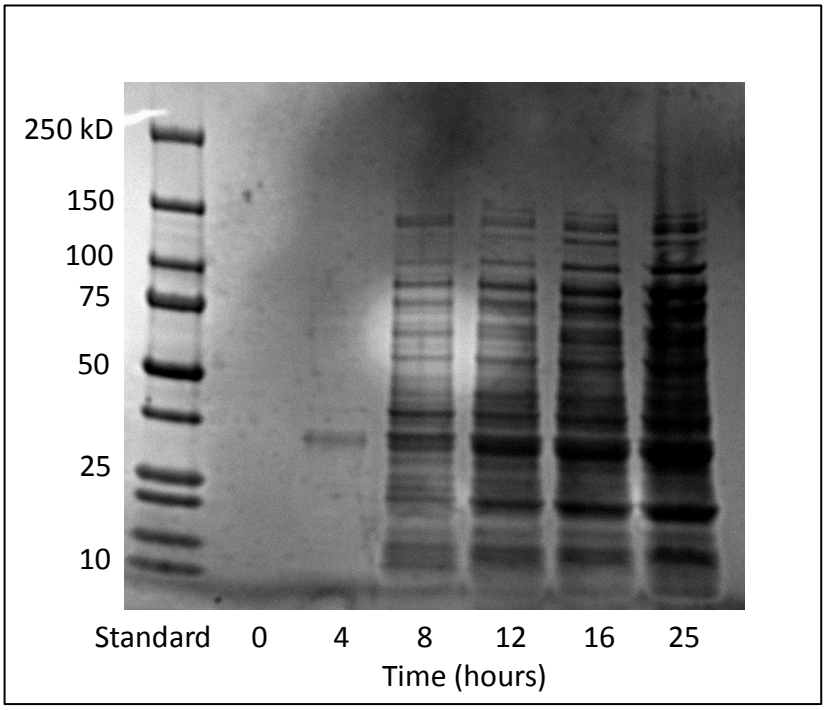

Figure 14 SDS-PAGE of the pET-41α empty vector. The columns are, from left to right, the Dual Color Protein Standards, empty, sample taken after 4 hours, sample taken after 8 hours, sample taken after 12 hours, sample taken after 16 hours, and a sample taken after 25 hours.

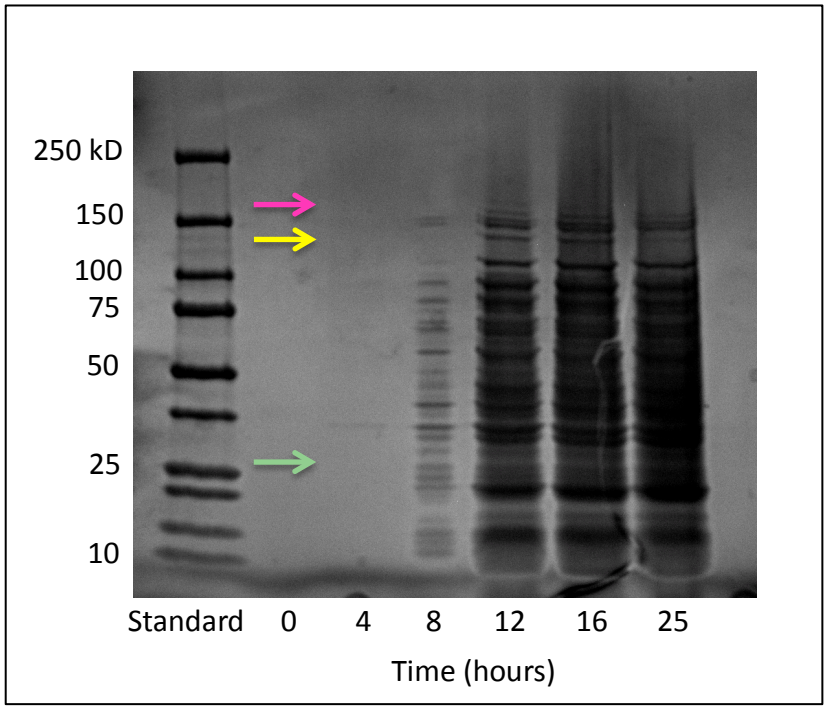

Figure 15 SDS-PAGE of the pET-41α vector with the *Sip1* insert. The columns are, from left to right, the Dual Color Protein Standards, empty, sample taken after 4 hours, sample taken after 8 hours, sample taken after 12 ours, sample taken after 16 hours, and a sample taken after 25 hours. The pink arrow represents the GST-tagged SIP1 protein. The yellow and green arrows represent SIP1 protein and the GST-tag, respectively.

Although the protein bands in general darken from left to right, denoting an increase in the amount of total protein, the SIP1 protein (136 kDa, yellow arrow in Figure 15) with a GST-tag (~26 kDa, green arrow), observable at ~166 kDa (pink arrow), should darken significantly more than the other proteins as its synthesis was specifically targeted by the IPTG induction. For reference, the uppermost band of the Protein Standard marks 250 kDa, and the band below that marks 150 kDa. As such, there is no obvious band that is the SIP1 protein. Further work is required to determine if the observed protein expression is from the expression vector itself or if it

is a result of the proteins found in *E. coli*, as well as for the identification, purification and characterization of the SIP1 protein. This will require performing a Western blot analysis with a GST antibody on the samples to confirm the presence or absence of the GST-tagged SIP1 protein and at what size it appears (to determine if the full SIP1 protein is being translated). Upon confirmation of the presence of SIP1 protein, the cytoplasmic, nuclear and membrane proteins must be separated with centrifugation techniques and analyzed with SDS-PAGE gel electrophoresis to determine the SIP1 protein's subcellular location. This will aid in further optimization of the initial conditions, leading to more efficient bulk production. Finally, the purified SIP1 protein will be obtained in bulk by utilizing the GST tag on the protein in conjunction with chromatography techniques. This work is not feasible for my remaining time at the University of Delaware.

Chapter 4

SPECIFIC AIM 2: CONFIRM AND IDENTIFY MIRNAS INVOLVED IN SIP1 EXPRESSION AND CONTROL

A knock out (KO) lacking SIP1 protein from the lens vesicle stage (E10.5) onward had already been established when I had joined the Duncan lab, and had been established to have lens development defects. Meanwhile, it had also been ascertained that SIP1 protein levels upregulate post-surgery in an EMT model. However, very little was known about the miRNAs in the normal or post-surgical lens, especially those involved in *Sip1* regulation, so this was a novel and critical experiment. I hypothesized that the miRNAs controlling *Sip1* expression are differentially regulated during development, as well as during PCO after cataract surgery, and that this differential gene expression is regulating *Sip1* function and thus affecting numerous downstream factors. I began experiments using reverse transcription (RT) and real-time (quantitative) polymerase chain reaction (qRT-PCR) techniques to determine if there are similar or additional feedback loops present between miRNAs and *Sip1* in the lens, and also to evaluate if the loss of *Sip1* has an effect on these miRNAs. In order to accomplish this, relative microRNA expression levels are measured and compared. RT methods are used to create complementary DNA (cDNA), which is then used in qRT-PCR to amplify the sequence, and detect the amount of cDNA as it is amplified. Ideally, the expression levels are normalized to an internal housekeeping gene that remains unchanged across all tissue samples, and then are compared to determine the fold change in the expression levels of the genes.

However, due to the novelty of the microRNAs in lens research, there are very few validated reference microRNA genes to use for normalization of expression levels (none of which have been used in our lab). It is necessary to control for error, which may be introduced at any step in the experimental protocol, between samples when measuring RNA expression, and one way to do this is by normalizing miRNA levels to an internal reference or housekeeping gene (Dheda *et al*, 2004). It is essential that the housekeeping gene be present in consistent levels throughout all biological samples, and because my study focuses on small RNAs, the gene of interest must be a small RNA as well.

In order to begin my investigation of miRNAs involved in PCO, I first had to identify and validate such a housekeeping gene that is also suitable to lens studies. I employed both a literature review (method 1) and experimental study (method 2) to determine and confirm one. Method 1 looked at available literature to find small RNAs, including both miRNAs and snoRNAs, that would be suitable to use as a housekeeping gene. I focused on small RNAs known to be involved in *Sip1* control, be present in the lens, be involved in development and/or be known for their housekeeping-gene characteristic. Several of these miRNAs and snoRNAs were chosen for the preliminary screening: miR200b, miR149, miR200b*, snoRNA234, snoRNA202 and miR205. As mentioned previously, the miRNA-200 family was shown to be involved in a double negative feedback loop with *Sip1* (Bracken *et al*, 2008). Reverse transcription and quantitative real-time PCR techniques were used to determine small RNA expression levels. To identify and validate a housekeeping small RNA gene whose expression levels did not change during experimental manipulations, adult wild type (WT) mice were compared to those of adult *Sip1* lens

knock out (KO) mice in both epithelial cells and fiber cells. All RNA samples used in this experiment to identify a housekeeping gene were previously prepared by Abby L. Manthey, a graduate student in the Duncan lab.

I identified that snoRNA202, a known housekeeping gene in mice (Recchiuti *et al*, 2010), was the best candidate for our housekeeping gene. snoRNAs, or small nucleolar RNAs, are similar to miRNAs in that they are small, non-protein coding RNAs (less than 400 nucleotides). They localize within the nucleolus, and associate with small nucleolar ribonucleoprotein particles (snoRNP), serving as their guide molecules during the post-transcriptional modification of ribosomal RNA (rRNA) and small nuclear RNA (snRNA). This modification often includes pseudouridylation and methylation of targeted RNA (Martens-Uzunova *et al*, 2013). snoRNA202 gave the most consistent and lowest C_T values (highest expression) throughout the cell types, and statistical f-tests and p-tests were performed showing that the values from the comparing cell type samples do not differ statistically. The data identifying snoRNA202 as the best housekeeping gene choice are shown below in *Table 1* with snoRNA202 values in blue, and in *Figure 16* as well. These figures denote that this small RNA has the most consistently low Ct values, which correspond to high expression levels. All in all, the outcome of method 1 and method 2 for determining a housekeeping gene matched.

Table 1 Housekeeping qRT-PCR Gene Analysis

Primer Set	**Epithelial Cells**		**Epithelial Cells +*cre***			
	Avg Ct	***Std Dev***	***Avg Ct***	***Std Dev***	***f value***	***P value (α=0.05, 1 tailed)***
*hsa miR200b**	38.5703	1.3116	38.0409	1.179	0.808	0.2216
hsa snoRNA234	27.5383	0.5482	27.3576	0.475	1.333	0.2543
hsa miR149	30.0226	0.7422	29.6560	0.144	26.450	0.0906
hsa miR200b	38.1550	0.9341	37.7416	0.801	1.359	0.2646
hsa snoRNA202	22.5275	0.4818	22.4538	0.376	1.641	0.3610
hsa miR205	38.0065	0.6764	34.8895	2.160	10.195	0.0021

Primer Set	**Fiber Cells**		**Fiber Cells +*cre***			
	Avg Ct	***Std Dev***	***Avg Ct***	***Std Dev***	***f value***	***P value (α=0.05, 1 tailed)***
*hsa miR200b**						
hsa snoRNA234	27.6699	0.6991	28.7873	0.6635	1.110	0.0016
hsa miR149	27.4021	0.3371	29.7926	0.4239	1.581	0.0000
hsa miR200b	37.2228	0.5822	38.0075	0.6378	1.200	0.0953
hsa snoRNA202	23.1970	0.3625	24.2018	0.7380	4.144	0.0017
hsa miR205	37.0967	0.7310	37.1428	2.0152	7.599	0.4769

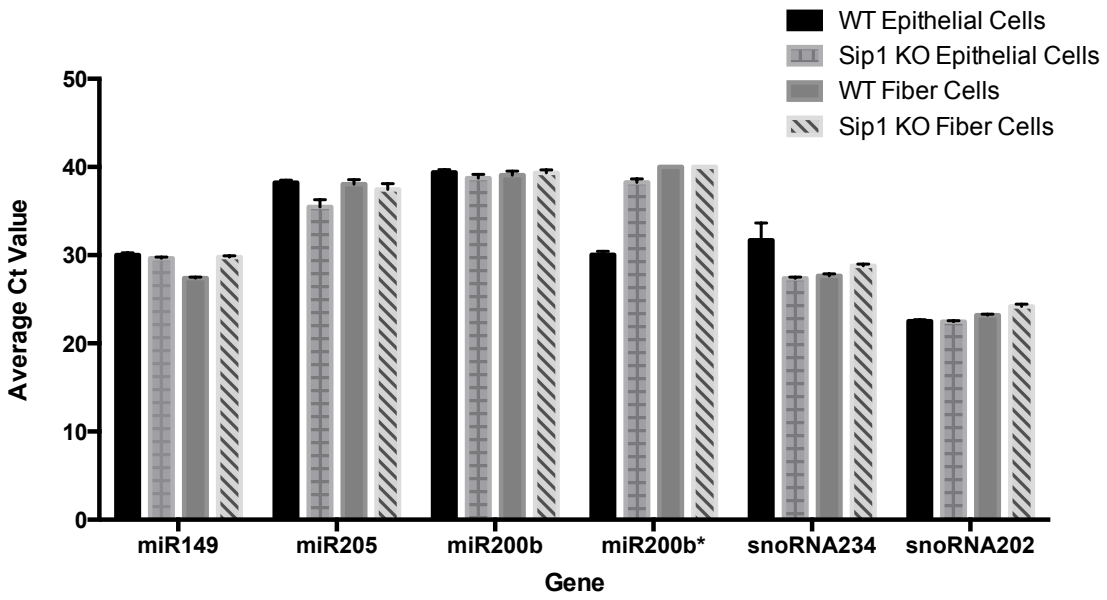

Figure 16 Small-RNA average Ct values for WT and *Sip1* KO RNA samples from epithelial cells and fiber cells of the lens. snoRNA202 is the only small-RNA to be found in consistent appreciable expression levels.

Next, I performed similar qRT-PCR experiments to investigate the expression pattern of the miR200 family in relation to SIP1 protein expression in PCO and during development to determine if this family of microRNAs does in fact regulate SIP1 protein expression during PCO. These family of miRNAs includes: miR141, miR200b, miR200b*, miR205 and snoRNA202. To determine miRNA expression during PCO I used Abby Manthey's 0hr post-surgery total RNA samples, and 48hr post-surgery total RNA samples. I focused on these two time points because 0hr post-surgery samples are a beginning time point when we would expect there to be reasonably high miRNA levels present, and 48hr post-surgery samples represent robust EMT (determined by the marker α-smooth muscle actin and the upregulation of SIP1 protein). The average Ct values, the fractional PCR cycle number at which the

reporter fluorescence is greater than the threshold, determined from six technical replicates of three biological samples are shown below in Figure 17.

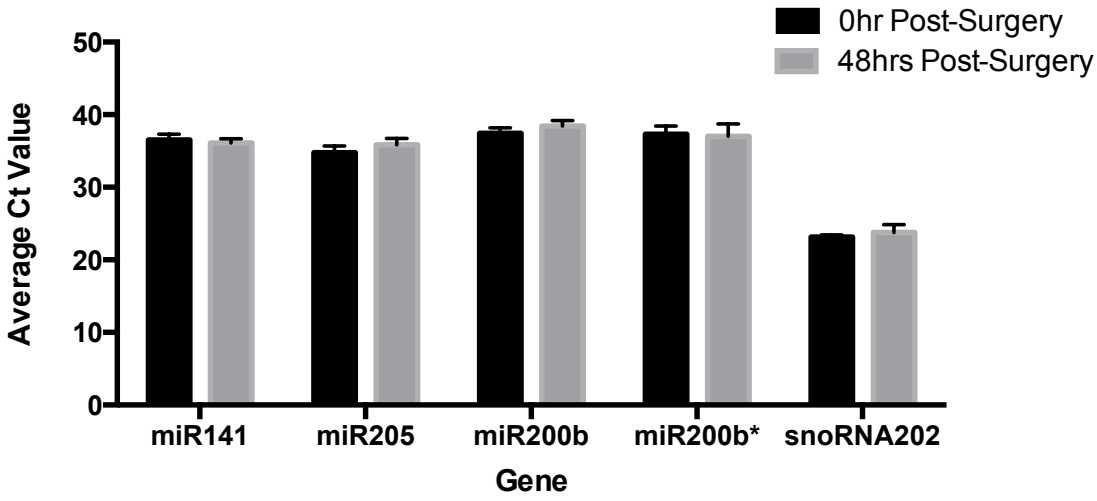

Figure 17 Average Ct Values For 0hr and 48hr Post-Surgery Sample miRNA Studies

As demonstrated by Figure 17, only snoRNA202 had an average Ct value below 30. Genes with average Ct values greater than 35 are not present in significant levels. Thus, these miRNAs of the miR200 family, miR141, miR205, miR200b, and miR200b* are not present in the lens, and are most likely not involved in the regulation of SIP1 protein expression during PCO. Additionally, no quantitative expression level changes were able to be determined for these miRNAs.

Next, expression levels of those same miRNAs in in embryonic tissue, namely, 15.5 dpc (days post conception) WT and KO samples were determined to identify possible miRNA regulators of *Sip1* during development. The average Ct

values determined from these data are given below in Figure 18. Once again, the housekeeping gene snoRNA202 had the greatest expression (as observed by a low Ct value), and miR141, miR200b, and miR200b* were not present in significant amounts as their average Ct values were equal or greater than 35. It is likely that these miRNAs are not involved in lens development. Finally, miR205 had an average Ct value of 30.68±0.16 in the WT sample, and an average Ct value of 30.62±0.23 in the KO sample. As the WT and KO average Ct values do not differ statistically, miR205 is most likely not differentially regulated by SIP1 during this stage of development, and it is unlikely that miR205 regulates Sip1.

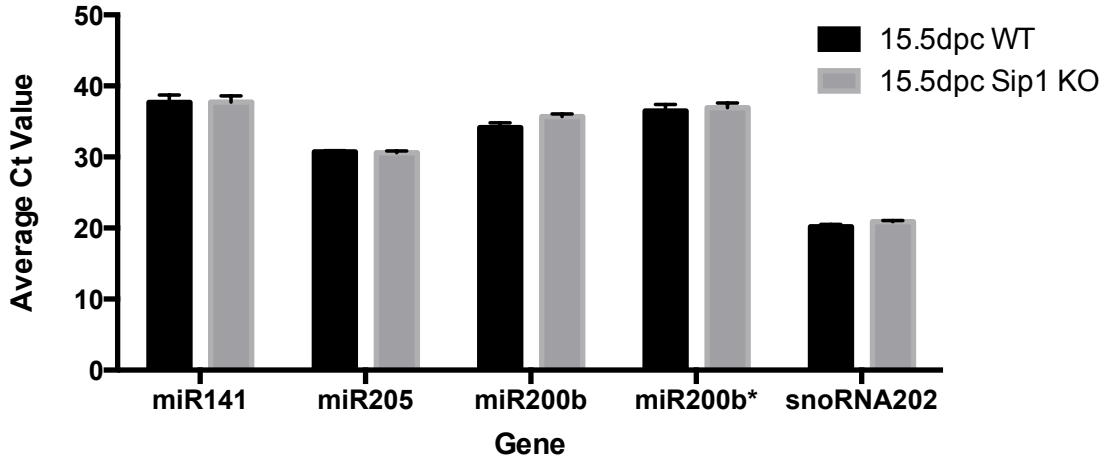

Figure 18 Average Ct Values For Embryonic Tissue miRNA Studies Using 15.5dpc *Sip1* KO and WT Total RNA Samples

After learning that the miR200 family double negative feedback loop with SIP1 is most likely not involved in PCO or development, I returned to the literature to identify other miRNAs that could play a role in lens development and/or PCO, and

found that miR31 is highly expressed in the lens. miR31 is a master regulator of development and wound healing processes, which include PCO (Karali *et al*, 2010). More specifically, miR31 was found to target multiple α integrin subunits, including α2, α5, and αV subunits. Expression of miR31 in cancer resulted in repression of these integrin subunits both at the mRNA and protein levels, which resulted in lack of cell spreading (Augoff *et al*, 2011). I hypothesized that miR31 could have a similar effect on αV subunits during PCO.

qRT-PCR using miR31 primers was performed on 13.5dpc WT kidney RNA samples, and 5 day total WT RNA samples to identify positive controls for this experiment. Only WT samples were studied in order to determine if miR31 was present in the lens in significant levels before further investigation ensued. Three technical replicates of one biological sample for the 5 day WT total RNA sample were performed because there were not enough samples for 3 biological samples. The average Ct value for miR31 expression in 13.5dpc WT kidney tissue was determined to be 32.03±0.24, and that in the 5 day WT lens cell RNA sample was 27.90±0.12. This experiment was repeated for 0hr post-surgery and 48hr post-surgery lens cell WT RNA samples to determine the expression pattern of miR31 during PCO. The average Ct value determined for 0hr WT lens cell RNA samples was 25.98±0.46, and that for 48hr WT lens cell RNA samples was 27.46±1.74. A p-value of 0.018 was determined for a t-test, showing that these data fall within 98% certainty. These values also correspond to a -2.66 fold change in the expression level of miR31. Thus, miR31 is downregulated in the PCO response in WT lenses.

Chapter 5

SPECIFIC AIM 3: INVESTIGATION OF MIR31 IN EMT

The finding that miR31 is downregulated during PCO in the WT lens led to the hypothesis that miR31 is involved in EMT, a crucial component of PCO. It had already been established (Fahmy Mamuya et al, manuscript in preparation) that αV integrin is involved in EMT, and a KO of αV integrin subunit will lack normal EMT behavior.

Because αV integrin subunit is involved in EMT, and miR31 is a known negative regulator of this integrin, I hypothesized that αV integrin subunit is negatively controlled by miR31. To begin validating this hypothesis I performed qRT-PCR with miR31 and the housekeeping gene snoRNA202 with 1 biological replicate of the following WT samples prepared by myself with graduate student Fahmy Mamuya: 0hr post-surgery, 24hr post-surgery, 48hr post-surgery and 5 day post-surgery lens cell RNA samples. 0hr post-surgery samples are still representative of normal lenses, 24hr post-surgery samples show the onset of PCO, 48hr post-surgery samples show robust PCO, and 5 day post-surgery samples show mature PCO. The average Ct values for miR31 only are given below in Figure 19.

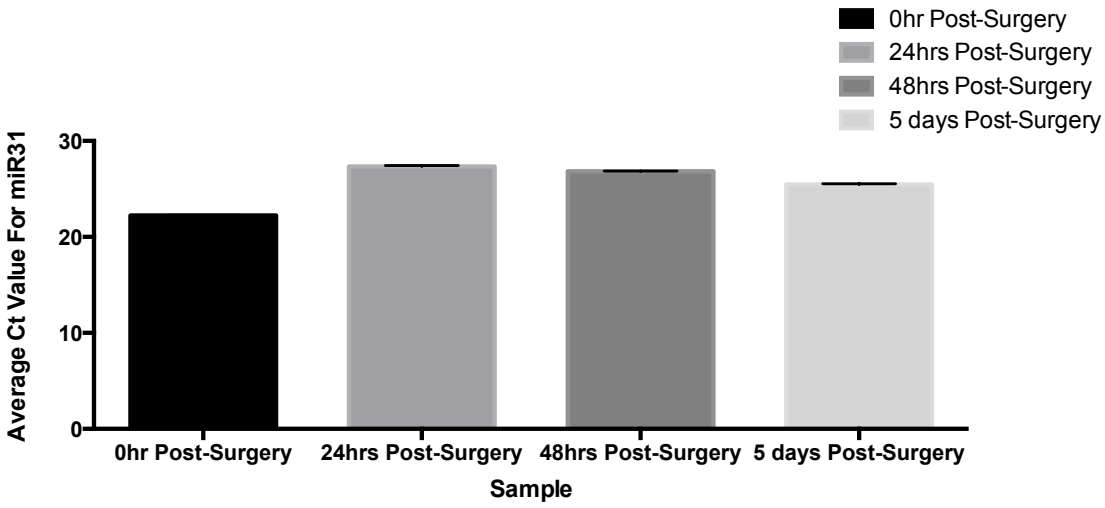

Figure 19 Average Ct Values For miR31 Expression Levels In 0hr, 24hr, 48hr, and 5 day post-surgery WT Lens Cell RNA Samples

As Figure 19 demonstrates, there is a decrease in miR31 expression at 24hrs post-surgery (as observed by a higher average Ct value), and then an increase in its expression at 48hrs and 5 days post-surgery (as seen by lower average Ct values). Because of the significant decrease in miRNA31 expression between 0hr post-surgery and 24hr post-surgery samples in the WT lens cells, further studies were performed with five biological replicates of WT 0hr and 24hrs post-surgery samples. The average Ct values for both miR31 and snoRNA202 are given below.

Table 2 Average Ct Values For miR31 and snoRNA202 In 0hr and 24hr WT Post-Surgery Samples

	miR31	*snoRNA202*
0hr	24.537 ± 2.07	23.456 ± 2.95
24hr	29.241 ± 1.09	26.914 ± 2.60

Additionally, the average fold changes in miR31 expression levels for the 24hrs post-

surgery sample, as well as for the 48hrs and 5 days post-surgery samples from the previous experiment, as compared to the 0hr post-surgery sample are presented in Figure 20. The value of -1.87±0.05 was determined for the 24hrs post-surgery fold change was found to be significant with a p value of 0.002.

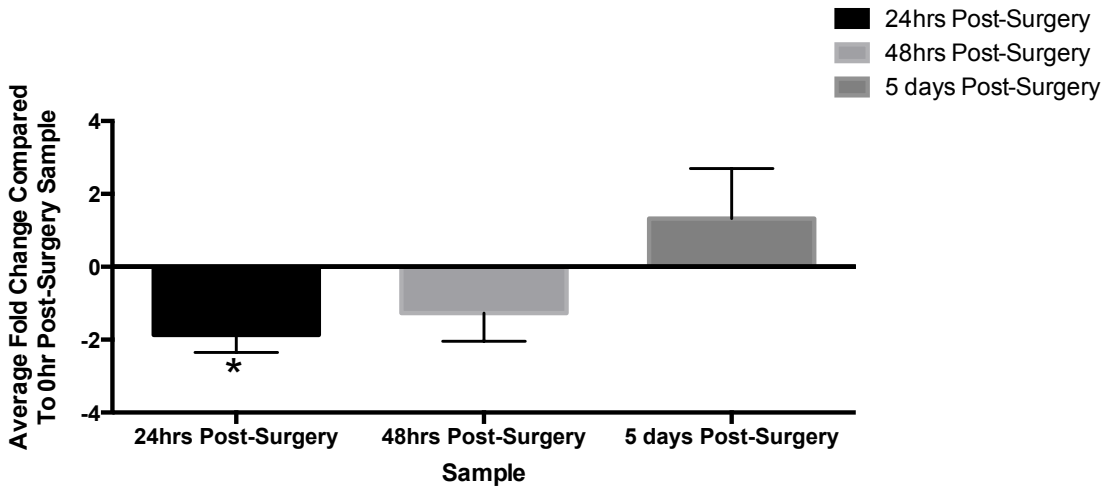

Figure 20 Average fold changes in miR31 expression levels in WT samples. *p=0.002.

Similar experiments with αV integrin subunit KO samples were performed, and the fold changes determined from these data are shown below in Figure 21, in addition to the WT expression fold change data from Figure 20.

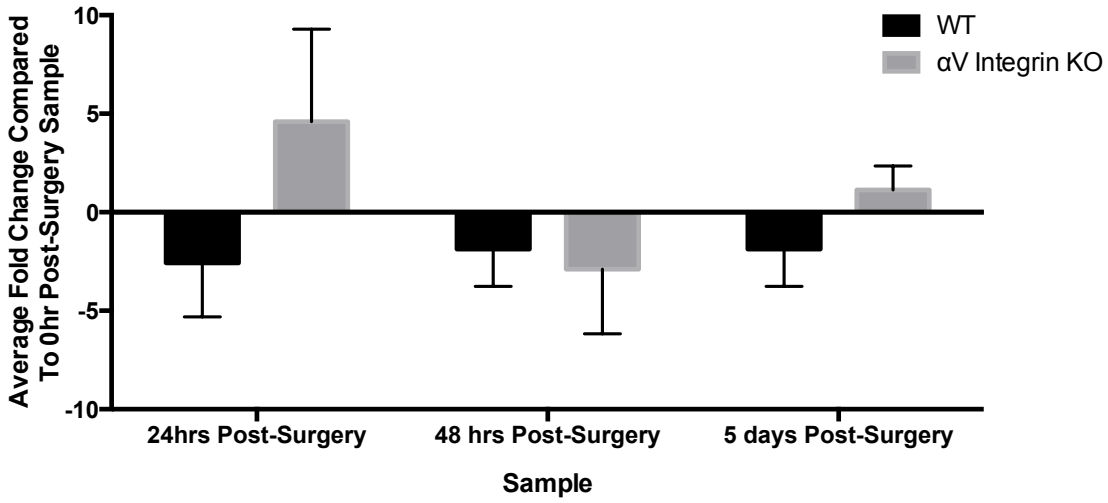

Figure 21 Average fold changes as compared to 0hr post-surgery samples for miR31 in both WT and KO lens cell samples. No p values were determined because 3 technical replicates were performed on only 1 biological replicate for the KO experiments.

Figure 21 demonstrates that the miR31 expression fold change is opposite in WT and KO samples at 24 hours post-surgery. This finding is consistent with the fact that WT samples beginning to under PCO at 24 hours post-surgery will have increased αV integrin subunit protein levels, and as such there will be less miR31 regulating them. KO samples do not undergo PCO, and will not need decreased miR31 levels to allow for an increase in αV integrin subunit.

Finally, a qRT-PCR experiment was performed with one biological replicate of 0 hour and 24 hours post-surgery WT and αV integrin subunit KO to determine the expression level of TGFβ-induced protein (TGFβi), which as described previously, is a component in EMT. The fold changes in *TGFβi* mRNA at 24 hours compared to the 0 hour WT value are given below in figure 22.

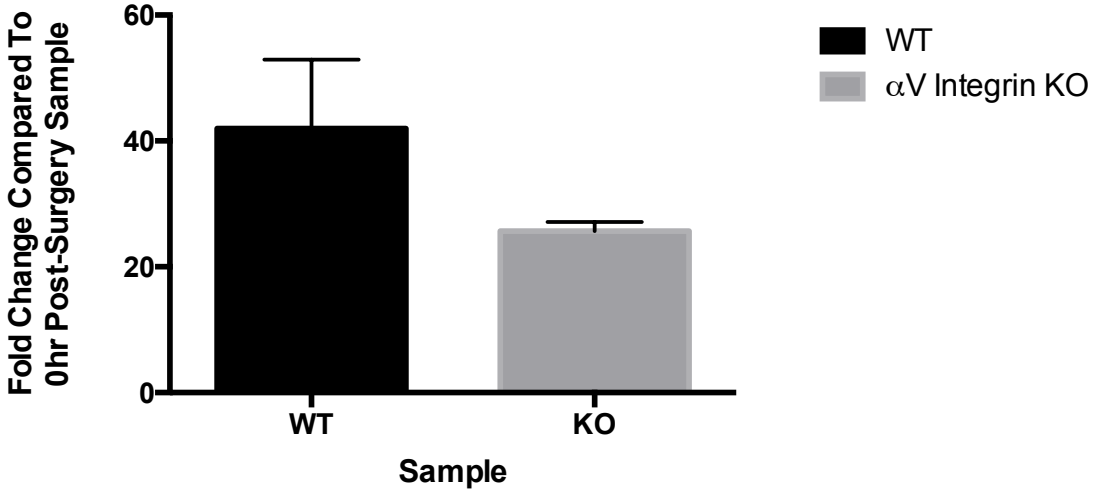

Figure 22 *TGFβi* mRNA expression fold changes in WT and KO 2 hour post-surgery samples compared to the 0 hour post-surgery WT sample. P values were not determined for only one biological replicate was used.

As observed in Figure 22, *TGFβi* mRNA levels decrease in the KO. This is consistent with the lack of PCO occurrence in the lens because TGFβi protein induces PCO, and is expected to present in higher levels in tissue with greater PCO. Similarly, αV integrin subunit KO lenses lack the αV integrin-TGFβ feed-forward loop and subsequent increased signaling, and there would be less TGFβi in the KO samples as a result.

As observed in Figures 19, 20 and 21, and in Table 2, all qRT-PCR experiments with miR31 are in agreement. miR31 expression levels decrease 24 hours post-surgery, and then increase again towards the level observed in 0hrs post-surgery samples at 48 hours and 5 days post-surgery. There is also a marked difference between the fold change in WT and that in KO samples at 24 hours post-surgery. This preliminary study suggests that miR31 may have a role in PCO.

Chapter 6

CONCLUSIONS AND FUTURE WORK

While lens extracapsular extraction has become the solution to cataract, the leading cause of blindness worldwide, it does not come without a price. Posterior capsular opacification (PCO), which often leads to the formation of a secondary cataract, is the major side effect of this surgery, affecting 50% of treated eyes. It is a mixed differentiation-wound healing process, involving both aberrant fiber cell differentiation and epithelial mesenchymal transition (EMT, Congdon *et al*, 2004), and the complete molecular mechanism remains elusive.

This study focused on two proteins known to upregulate during the PCO phenomena: Smad-interacting protein 1 (SIP1), and αV intregrin. The work involving SIP1 remains inconclusive. A pET-41a(+)-*Sip1* expression vector was successfully created. However, further experiments need to be performed in order to express, identify and purify SIP1 protein, which can then be used to create an anti-Sip1 antibody. miRNA studies using qRT-PCR techniques identified snoRNA202 as an appropriate housekeeping gene, or internal reference, for miRNA expression level studies in the lens. Furthermore, the miRNAs of the miR200 family were not present in appreciable levels in the lens. Thus, it is most likely that the double-negative feedback loop between those miRNAs and *Sip1* known to control cell phenotype in multiple cell types, including cancerous ones, is not involved in PCO.

miRNA expression studies during PCO continued as two pieces of information became apparent. First, αV integrin showed upregulation at the protein level, but not

at the RNA level, suggesting that αV integrin is not under transcriptional control during EMT. Secondly, it was published that miR31 is a master regulator of αV integrin that can control its translation (Augoff *et al*, 2011). Subsequent miR31 studies showed a significant fold change of -1.87±0.05 in 24 hours post-surgery WT lens cell samples. Interestingly, that of the 24 hours post-surgery KO lens cell samples, in which PCO is absent, was 1.14±0.07, almost the absolute value of that of the WT value. This showed that miR31 is indeed downregulated during the onset of PCO.

Similar miRNA studies were performed for TGFβi, the induced protein form of TGFβ, in both WT and KO lens cell samples. The fold changes were calculated for 24 hours post-surgery samples as compared to their respective 0 hour post-surgery samples. The fold change of the WT was 41.97±10.96, and that of the KO was 25.66±1.49. The lesser fold change in the KO is consistent with the fact that there is no PCO in these samples. Ultimately, these findings led to a proposed model, shown below in Figure 21, for miR31 involvement in PCO.

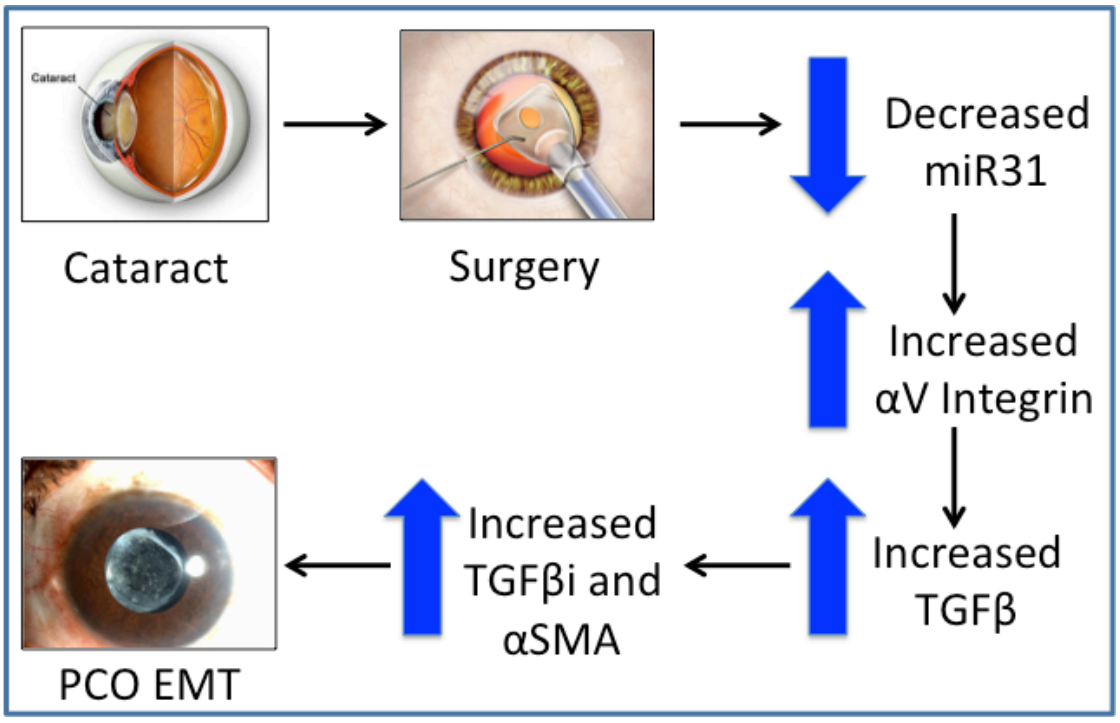

Figure 23 Proposed model for miR31 involvement in PCO. In the event of surgery, miR31 downregulates, allowing for increased expression of αV integrin subunit protein. Increased αV integrin subunit participates in a feed forward loop to augment TGFβ levels, which then induces production of TGFβi and αSMA proteins. Finally, TGFβi protein is known to stimulate EMT.

In order to test this model, some future studies of this project include creating a KO for the *miR31* gene in mice, performing transfection experiments with known negative inhibitors of miR31 to confirm corresponding downstream effects, and upregulating miR31 in cells that have already undergone EMT to determine the extent

of miR31 control during PCO. Alternative methods to specifically designed to isolate miRNAs, such as the mirVana^{TM} miRNA Isolation Kit, can be used to ensure that the maximum amount of miRNA is being isolated, and that these miR amounts correspond to the current findings. Additionally, SIP1 protein purification studies can be modified such that the unique structural components of SIP1 protein can be ultilized.

While the complete mechanism of PCO is highly complicated and remains unresolved, this study may provide a piece of the puzzle. Further studies involving miR31 expression throughout processes such as eye development, cataract formation, and PCO must be performed to better ascertain it role. Understanding the molecular basis of eye development, cataracts and wound healing is essential to the world of ophthalmology. It is especially important because of the prevalence of cataract worldwide, and the occurrence rate of PCO in those who are treated. Nevertheless, because of the complex nature of PCO, and its dual developmental-would healing process, this study is beneficial to lens biology as a whole, and could serve as a foundation for future studies, which may eventually achieve miRNA treatment of PCO.

REFERENCES

Andersen H, Berx G, Bruyneel E, Comijn J, De Craene B, Tulchinsky E, Van Roy F, Vandewalle C, and Vermassen P (2005) SIP1/ZEB2 EMT by repressing genes of different epithelial cell-cell junctions. *Oxford Journals*. **33**, 6566-6578.

Andley AP (2007) Crystallin in the eye: function and pathology. *Progress in Retinal and Eye Research.* **26**, 78-98.

Andley UP (2008) The lens epithelium: Focus on the expression and function of the α-crystallin chaperones. *The International Journal of Biochemistry & Cell Biology*. **40**, 317-323. http://dx.doi.org/10.1016/j.biocel.2007.10.034.

Augoff K, Das M, Bialkowska K, et al (2011) miR-31 Is a Broad Regulator of β1-Integrin Expression and Function in Cancer Cells. *Molecular Cancer Research*. **9**, 1500-1508. doi:10.1158/1541-7786.MCR-11-0311

Barraquer RI, Michael R, Abreu R, Lamarca J, Tresserra F (2006) Human lens capsule thickness as a function of age and location along the sagittal lens perimeter. *Invest. Ophthalmol. Vis. Sci.* **47**, 2053-2060.

Bartel DP (2004) MicroRNAs: Genomics, biogenesis, mechanism, and function. *Cell* **116**, 281-297.

Bassnett S, Missey H, Vucemilo I (1999) Molecular architecture of the lens fiber cell basal membrane complex. *J. Cell Sci.* **112**, 2155-2165.

Blakely EA, Bjornstad KA, Chang PY, McNamara MP, Change E, Aragon G, Lin SP, Lui G, Polansky JR (2000) Growth and differentiation of human lens epithelial cells in vitro on matrix. *Invest. Ophthalmol. Vis. Sci.* **41**, 3898-3907.

Beebe DC, Vasiliev O, Guo J, Shui YB, Bassnett S (2001) Changes in adhesion complexes define stages in the differentiation of lens fiber cells. *Invest. Ophthalmol. Vis. Sci*. **42**, 727-734.

Benedek G (1971) Theory of the transparency of the eye. *Appl. Optics* **10**, 459-473.

Benedek G (1983) Why is the eye lens transparent?. *Nature* **302**, 383-384.

Beyer TL, Vogler G, Sharma D, O'Donnell Jr FE (1984) Protective barrier effect of the posterior lens capsule in exogenous bacterial endophthalmitis-an experimental primate study. *Invest. Ophthalmol. Vis. Sci.* **25**, 108-112.

Bhat SP (2001) The ocular lens epithelium. *Biosci. Rep*. **21**, 537-563.

Bhat SP, and Nagineni CN (1989) alpha B subunit of lens-specific protein alpha-crystallin is present in other ocular and non-ocular tissues. *Biochem. Biophys. Res. Commun*. **158**, 319-325.

Boyle DL, Takemoto L, Brady JP, Wawrousek EF (2003) Morphological characterization of the Alpha A- and Alpha B-crystallin double knockout mouse lens. *BMC Ophthalmol*. **3**, 3.

Bracken CP, Gregory PA, Kolesnikoff N, Bert A, Wang Y, Shannon MF, and Goodall GJ (2008) A Double-Negative Feedback Loop between ZEB1-SIP1 and the microRNA-200 Family Regulates Epithelial-Mesenchymal Transition. *Cancer Res* **68**, 7846-7854.

Bushlin I, Devi L, Gomes I, Gupta A, Hipser C (2010). Role of Antibodies In Developing Drugs That Target G-Protein-Coupled Receptor Dimers. *Mount Sinai Journal of Medicine: A Journal of Translational and Personalized Medicine*. **77**, 374-380.

Cammarate P, Cantu-Crouch D, Oakford L, Morrill A (1986) Macromolecular organization of bovine lens capsule. *Tissue Cell*. **18**, 83-97.

Chiu C (2008) "Cataract Surgery in the 21st Century" UCSF Mini Medical School. The UCSF Osher Center for Integrative Medicine. University of California, San Francisco.

Clark, DS (2000) Posterior capsule opacification. *Curr Opin Ophthalmol*. **11**, 56-64.

Comijn J, Berx G, Vermassen K, van Grunsyen L, Bruyneel E, Mareel M, Huylebroeck D, van Roy F (2001) The two-handed E box binding zinc finger protein SIP1 downregulates E-cadherin and induces invasion. *Mol. Cell*. **6**, 1267-78.

Congdon N, O'Colmain B, Klaver CC, Klein R, Muñoz B, Friedman DS, Kempen J, Taylor HR, Mitchell P, Eye Diseases Prevalence Research Group (2004) Causes and prevalence of visual impairment among adults in the United States. *Archives of Ophthalmology* **122**, 477-485.

Coulombre AJ (1979) Cataractogenesis: developmental inputs and constraints. *Ophthalmology* **86**, 1559-1570.

Danysh BP, and Duncan MK (2009) The lens capsule. *Experimental Eye Research* **88**, 151-164.

Dheda K, Huggett JF, Bustin SA, Johnson MA, Rook G, and Zumla A (2004) Validation of housekeeping genes for normalizing RNA expression in real-time PCR. *BioTechniques* **37**, 112-199.

Fisher RF, and Pettet BE (1972) The postnatal growth of the capsule of the human crystalline lens. *J. Anat.* **112**, 207-214.

Friedenwald J (1930a) The permeability of the lens capsule to water, dextrose, and other sugars. *Arch. Ophthalmol*. **4**, 350-360.

Friedenwald J (1930b) Permeability of the lens capsule with special reference to the etiology of senile cataract. *Arch Ophthalmol*. **3**, 182-193.

Hansen TB, Bramsen JB, Kjems J (2010) Re-Inspection of small RNA sequence datasets reveals several novel human miRNA genes. *PLoS ONE* 5(6): e10961. doi:10.1371/journal.pone.0010961

Grabitz AL, Duncan MK (2010) Focus on Molecules: Smad Interacting Protein 1 (Sip1, ZEB2, ZFHX1B), *Experimental Eye Research* doi: 10.1016/j.exer.2010.09.010.

Gregory PA, Bracken CP, Bert AG, Goodall GJ (2008) MicroRNAs as regulators of epithelial-mesenchymal transition. *Cell Cycle* **7:20**, 3112-3118.

Hales AM, Schulz MW, Chamberlain CG, McAvoy JW (1994) TGF-beta1 induces lens cells to accumulate alpha-smooth muscle actin, a marker for subcapsular cataracts. *Curr. Eye Res.* **13**, 885-890.

Higashi Y, Kondoh H, Saigou Y, Yoshimoto A (2005). Regulation of ocular lens development by Smad-interacting protein 1 involving Foxe3 activation. *Development.* **132**, 4437-4448.

Horwitz J (1992) Alpha-crystallin can function as a molecular chaperone. *Proc. Natl. Acad. Sci. USA* **89**, 10449-10453.

"IPTG, Dioxane-Free." *www.promega.com*. Promega Corporation, 2012. Web. 24 Feb. 2012. <http://www.promega.com/products/biochemicals-and-labware/biochemical-buffers-and-reagents/iptg_-dioxane_free/>.

Karali M, Peluso I, Gennarino VA, Bilio M, Verde R, Lago G, Dollé P, Banfi S (2010) miRNeye: a microRNA expression atlas of the mouse eye. *BMC Genomics* **11**, 715-727.

Kuzak JR, and Brown HG (1994) Embryology and anatomy of the lens. In *Principles and Practice of Ophthalmology* (D. M. Alberts and F. A. Jakobiec, eds) pp. 82-96. W.B. Saunders, Philadelphia.

Land MF (1988) The optics of animal eyes. *Contemp. Phys*. **29**, 435-455.

Land MF, and Fernald RD (1992) The evolution of eyes. *Annu. Rev. Neurosci*. **15**, 1-29.

Lang RA (2004) Pathways regulating lens induction in the mouse. *International Journal of Developmental Biology* **48**, 783-791.

Li Y, and Piatigorsky J (2009) Targeted deletion of Dicer disrupts lens morphogenesis, corneal epithelium stratification, and whole eye development. *Developmental Dynamics* **238**, 2388-2400.

Mamuya FA, and Duncan MK (2012) αV Integrins and TGFβ Induced EMT; a Circle of Regulation. *J Cell Mol Med.* **16**, 445-455. doi:10.1111/j.1582-4934.2011.01419.x.

Martens-Uzunova ES, Olvedy M, and Jenster G. (2013) Beyond microRNA – Novel RNAs derived from small non-coding RNA and their implication in cancer, Cancer Lett http://dx.doi.org/10.1016/j.canlet.2012.11.058

Mousa SA (2003) αV vitronectin receptors in vascular-mediated disorders. *Medicinal Research Reviews*. **23**, 190-199. doi 10.1002/med.10031

Park SM, Gaur AB, Lengyel E, Peter ME (2008) The miR-200 family determines the epithelial phenotype of cancer cells by targeting the E-cadherin repressors ZEB1 and ZEB2. *Genes Dev* **22**, 894-907.

Piatigorsky J (1981) Lens differentiation in vertebrates. A review of cellular and molecular features. *Differentiation* **19**, 134-152.

Piatigorsky J (1998) Multifunctional lens crystallins and corneal enzymes. More than meets the eye. *Ann. N Y Acad. Sci.* **842**, 7-15.

Piatigorsky J (2008) Gene sharing in lens and cornea: facts and implications. *Progress in Retinal and Eye Research* **17**, 145-174.

Recchiuti A, Krishnamoorthy S, Fredman G, Chiang N, and Serhan CN. (2010) MicroRNAs in resolution of acute inflammation: identification of novel D1-miRNA circuits. *The FASEB Journal*. **25**, 544-560.

Saika S, Okada Y, Miyamoto T, Ohnishi Y, Ooshima A, McAvoy JW (2001) Smad translocation and growth suppression in the lens epithelial cells by endogenous TGFbeta2 during wound repair. *Exp. Eye Res.* **72**, 679-686.

Shaham O, Smith A, Robinson M, Taketo M, Lang R, Ashery-Padan R (August 2009) Pax6 is essential for lens fiber cell differentiation. *Development*. **136**, 2567-2578. doi: 10.1242/dev.032888.

Sheppard D (2004) Roles of αv integrins in vascular biology and pulmonary pathology. *Current Opinion in Cell Biology*. **16**, 552-557. doi: 10.1016/j.ceb.2004.06.017

Spalton D (2011) Preventing PCO. *EyeWorld Online*. ASCRS Ophthalmic Services Corp.

Steinberg EP, Javitt JC, Sharkey PD, *et al.* (1993) The content and cost of cataract surgery. *Arch. Ophthalmol.* **111**, 1041-1049.

Thim K, Krag S, Corydon L (1991) Stretching capacity of capsulorhexis and nucleus delivery. *J. Cataract. Refract. Surg.* **17**, 27-31.

Thim K, Krag S, Corydon L (1993) Hydroexpression and viscoexression of the nucleus through the continuous circular capsulorhexis. *J. Cataract. Refract. Surg*. **19**, 209-212.

Vandewalle C, Comijn J, De Craene B, Vermassen P, Bruyneel E, Andersen H, Tulchinsky E, Van Roy F, Berx G (2005) Sip1/Zeb2 induces EMT by repressing genes of different epithelial cell-cell junctions. *Nucleic Acids Research*. **33**, 6566-6578.

Vandewalle C, Van Roy F, and Berx G (2009) The role of the ZEB family of transcription factors in development and disease. *Cell Mol. Life Sci.* **66**, 773-787.

Weiss SM, and Cheresh DA (2011) αv Integrins in Angiogenesis and Cancer. *Cold Spring Harb Perspect Med*. 1-14. doi: 10.1101/cshperspect.a006478

Wormstone IM, Wang L, and Liu CS (2009) Posterior capsule opacification. *Exp Eye Res* **88**, 257-269.

Yoshimoto A, Saigou Y, Higashi Y, and Kondoh H (2005) Regulation of ocular lens development by Smad-interacting protein 1 involving *Foxe3* activation. *Development* **132**, 4437-4448. doi:10.1242/dev.02022.

Zampighi GA, Eskandari S, and Kremen M (2000) Epithelial organization of the mammalian lens. Exp. Eye Res. **71**, 415-435.

Zweier C, et al. (2005) Clinical and mutational spectrum of Mowat-Wilson syndrome. *Eur. J. Med. Genet.* **48**, 97-111.